Fermi National Accelerator Laboratory

FERMILAB-Conf-90/256-E
[E-741/CDF]

Results from Hadron Colliders *

The CDF Collaboration

presented by

Lee G. Pondrom
University of Wisconsin
Madison, Wisconsin 53706

December 14, 1990

* To be published in the proceedings of the XXVth International Conference on High Energy Physics, Kent Ridge, Singapore, August 2-8, 1990.

Fermilab-CONF-90/256-E
CDF/PUB/CDF/PUBLIC/1330
December 14, 1990

RESULTS FROM HADRON COLLIDERS

LEE G. PONDROM
University of Wisconsin
Madison, Wisconsin, USA

Abstract

The present status of hadron collider physics is reviewed. The total cross section for $\bar{p}+p$ has been measured at 1.8 TeV: $\sigma_{\rm tot} = 72.1 \pm 3.3$ mb. New data confirm the UA2 observation of $W/Z \to \bar{q}q$. Precision measurements of M_W by UA2 and CDF give an average value $M_W = 80.13 \pm 0.30$ GeV/c^2. When combined with measurements of M_Z from LEP and SLC this number gives $\sin^2\theta_W = 0.227 \pm 0.006$, or $m_{\rm top} = 130^{+40}_{-60}$ GeV/c^2 from the EWK radiative correction term Δr. Evidence for hadron colliders as practical sources of b quarks has been strengthened, while searches for t quarks have pushed the mass above M_W: $m_{\rm top} > 89$ GeV/c^2 95% cl (CDF Preliminary). Searches beyond the standard model based on the missing E_T signature have not yet produced any positive results. Future prospects for the discovery of the top quark in the range $m_{\rm top} < 200$ GeV/c^2 look promising.

1 Low p_t Cross Sections

1.1 *Total $\bar{p}p$ cross section at 1.8 TeV*

A new luminosity independent measurement of the $\bar{p}p$ total cross section has been reported by the E710 group at Fermilab [1]. In the experiment the differential yield $dN_{\rm el}/dt$ for elastic scattering and the number of inelastic events $N_{\rm inelas}$ were measured simultaneously. Drift chambers triggered by scintillation counters in moveable "Roman pots" at 25 m and 91 m from the crossing point measured the coordinates of elastically scattered $\bar{p}$'s, while similar detectors at 25 m and 121 m measured the p's [2]. The inelastic events were recorded by rings of scintillation counters at larger angles. One formula for the total cross section is given by the extrapolation of $dN_{\rm el}/dt$ to the optical point at $t = 0$:

$$\sigma^2_{\rm tot} = \frac{(16\pi dN_{\rm el}/dt)_{t=0}}{(1+\rho^2)L} \ , \qquad (1)$$

where $\rho = {\rm Re}(f(0))/{\rm Im}(f(0))$, $f(0)$ being the forward elastic scattering amplitude, and L the integrated luminosity. ρ is expected to be much less than unity. A second formula for the total cross section comes from the total number of inelastic events:

$$\sigma_{\rm tot} = (N_{\rm el} + N_{\rm inel})/L \ . \qquad (2)$$

Since Eqs. (1) and (2) have different dependence of $\sigma_{\rm tot}$ on L, the integrated luminosity can be eliminated from the total cross section expression:

$$\sigma_{\rm tot} = \frac{(16\pi dN_{\rm el}/dt)_{t=0}}{(1+\rho^2)(N_{\rm el}+N_{\rm inel})} \qquad (3)$$

Here $\sigma_{\rm tot}$ depends inversely on $(1+\rho^2)$. The total cross section in Eq. (1) is not as sensitive to ρ, depending only on $(1+\rho^2)^{1/2}$, but it involves the less well known integrated luminosity L [3].

There is some uncertainty regarding the value of ρ to be substituted into Eq. (3), since a coulomb interference measurement at 1.8 TeV has not been reported. The highest energy published value for ρ was obtained at the CERN SPS at 546 GeV [4]:

$$\rho = 0.24 \pm 0.04 \qquad 546 \text{ GeV}. \qquad (4)$$

Block and Cahn [5] give a general review of the various models used to describe elastic scattering. In particular, they expressed [5, 6] the forward scattering amplitudes as analytic functions of $s = E^2_{\rm tot} - \vec{p}^2_{\rm tot}$ with eight arbitrary parameters. Values for the parameters have been obtained by fitting the functions to the $\bar{p}p$ data up to 900 GeV [6]. These fits to data above 15 GeV when extrapolated to 1.8 TeV give a range of possible cross sections between 75 mb and 81 mb, with ρ values between 0.09 and 0.14 respectively. Larger cross sections are correlated in general with larger values of ρ. In the absence of experimental data, the value

$$\rho = 0.145 \qquad 1.8 \text{ TeV} \qquad (5)$$

was assumed in Ref. [1], leading to a total cross section

$$\sigma_{\rm tot} = 72.1 \pm 3.3 \text{ mb at } 1.8 \text{ TeV}. \qquad (6)$$

Pub. Proceedings 25th International Conference on High Energy Physics, Singapore, August 2-8. 1990

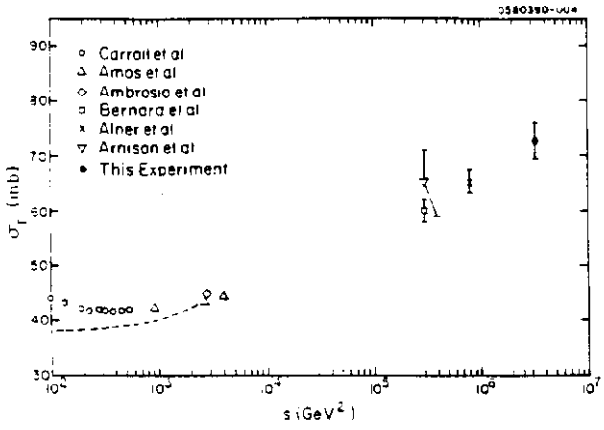

Figure 1a: Measurements of the total cross section for $\bar{p} + p$ as a function of s taken from Ref [1]. The dashed line is the pp total cross section.

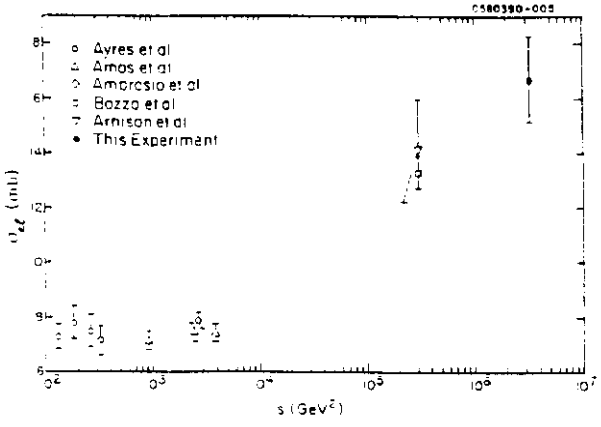

Figure 1b: Measurements of the elastic cross section for $\bar{p} + p$ as a function of s taken from Ref [1].

and an elastic cross section

$$\sigma_{\rm elas} = 16.6 \pm 1.6 \text{ mb at } 1.8 \text{ TeV}. \qquad (7)$$

The errors quoted in Eq. (6) are statistical. If ρ is taken from Eq. (4), then $\sigma_{\rm tot} = 69.6 \pm 3.2$ mb. The total and elastic cross section points on a plot *vs* s are shown in Figs. 1a and 1b. The slope of the elastic cross section used for the optical point extrapolation is shown in Fig. 2 [7].

The data are in reasonable agreement with the extrapolations of Ref. [5], and also with the impact picture model of Bourrely *et al* [8]. The ρ value has to be supplied from theory. A measurement of ρ at 1.8 TeV would be very desirable. It will be interesting to obtain high energy pp data to compare to

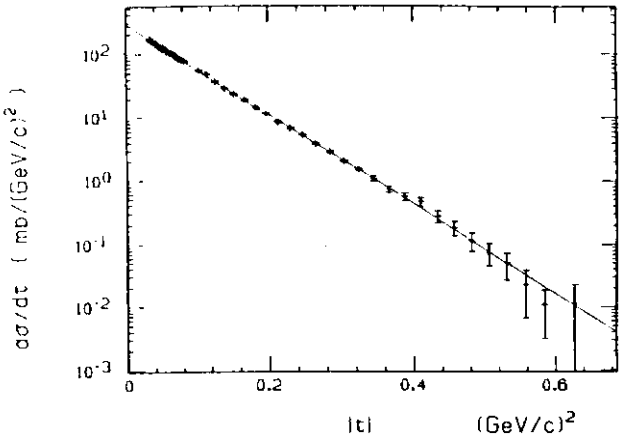

Figure 2: Elastic slope for $\bar{p} + p$ at 1.8 TeV taken from Ref [7]. The straight line is a fit of the form A exp (Bt) in the range $0.034 < |t| < 0.65$.

the $\bar{p}p$ cross section in this more nearly asymptotic region.

1.2 *Pomeron Exchange*

The Pomeron is a relic of the phenomenology of Regge poles. A wide variety of small angle scattering phenomena was explained in the 1960's by the Regge pole picture, in which scattering and reactions were described in terms of the exchange of "particles"—Regge trajectories—in the t channel which had fixed quantum numbers such as I spin, but continuously variable spin angular momentum [9]. The trajectory with the quantum numbers of the vacuum was called the Pomeron in honor of I. Ya. Pomeranchuk, who made many contributions to the description of high energy scattering long before even $\sqrt{s} = 10$ GeV was achieved in the laboratory [10].

Pomeron exchange is thought to play a role in small angle $\bar{p}p$ reactions through single diffraction, double diffraction, and double Pomeron exchange. See Figs. 3a, b, and c. These processes can be distinguished by kinematics. Thus in Fig. 3c the inelastically produced particles are in the central region, at rest in the collider frame, while the particles in Figs. 3a and b are moving with the projectile. These processes remain an active field of collider research. In Ref. [1] the authors quote a value for the single diffraction process of Fig. 3a based on analysis of the single arm ring scintillator events, in which the diffractive debris was detected, but not the unper-

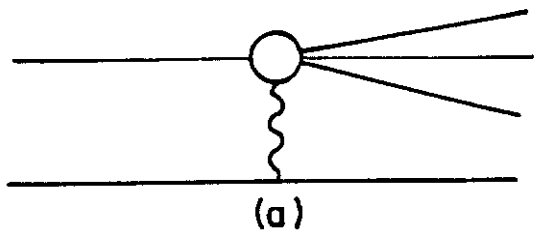

Figure 3a: Single diffractive excitation by Pomeron exchange. The decaying system has the quantum numbers of the proton (or $\bar{p}$).

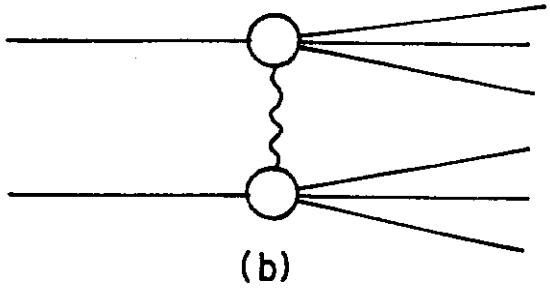

Figure 3b: Double diffractive excitation by Pomeron exchange.

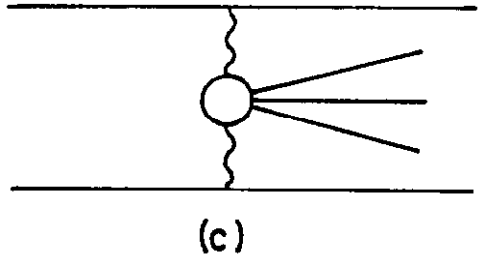

Figure 3c: Double Pomeron exchange, leading to the creation in the central region of states with vacuum quantum numbers.

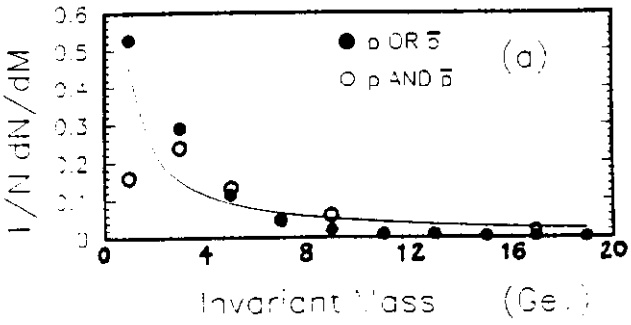

Figure 4a: Invariant mass of D-P exchange events from Ref [11]. Either the recoil p or $\bar{p}$ was detected (closed circles), or both were (open circles).

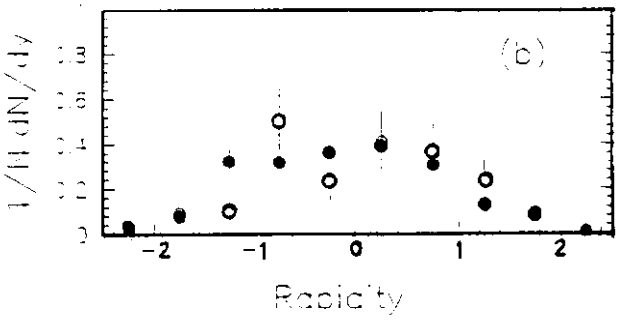

Figure 4b: Rapidity distribution of the detected excited state in the central region. Open and closed circles have the same meaning as in 4a.

turbed $p/\bar{p}$ which remained in the beam pipe. Their result is:

$$\sigma_{SD} = 11.7 \pm 2.3 \text{ mb at } 1.8 \text{ TeV}. \qquad (8)$$

Brandt *et al* [11] reported to this conference a measurement of double Pomeron exchange (Fig. 3c) at the CERN SPS at 630 GeV. Isolation and study of this reaction could lead to information regarding new objects with vacuum quantum numbers, for instance glue balls. Wire chambers in four Roman pot spectrometers were used to measure the p and $\bar{p}$ trajectories, and the UA2 detector registered the energy flow of particles produced in the central region. The threshold transverse momenta for the p and $\bar{p}$ triggers were 1 GeV/c. The invariant mass and rapidity distributions for 121 events where both the p and $\bar{p}$ were detected (open circles), and 1286 where only one was detected (closed circles) are shown in Figs. 4a and 4b. The invariant mass was calculated from

UA2 calorimeter data assuming massless particles interacted in the calorimeter towers. The single arm data were corrected for single diffraction contamination. The average mass observed for double pomeron exchange was about 3 GeV. A preliminary estimate of a cross section for this process is 30–150 μbarn.

1.3 *Multiplicity, Clustering, etc.*

The considerable activity at the Conference on these subjects is covered in the review by Wroblewski [12].

2 JETS

The majority of recent activity in jets and QCD at hadron colliders is covered in the review by Jacob [13]. This section will report on a study of the invariant mass of di-jets in the region between 50 and 100 GeV/c^2 at 630 GeV. A study of this mass region based on earlier SPS collider data has been published [14]. The 1988-89 run with 7.4 pb^{-1} integrated luminosity has considerably improved the statistical power of this analysis.

Prime interest in this di-jet mass region comes not from the QCD continuum, but rather from the signal of $q\bar{q}$ decays of W and Z intermediate bosons. At 630 GeV the peaks from $W \rightarrow q\bar{q}$ and $Z \rightarrow q\bar{q}$ smeared by detector resolution are 1/100 of the QCD continuum. It is an experimental challenge to extract a useful signal. The reward is not only a check of the expectations of the standard model for W and Z decays, but also an existence proof to motivate the construction of better jet invariant mass resolution calorimeters. Many signatures of new physics at higher energies involve anomalous production of W and Z bosons. If the $q\bar{q}$ final states can be detected, then a larger acceptance for bosons is achieved because of the large $q\ \bar{q}$ branching ratio, and an otherwise missing constraint on the invariant mass is obtained for W's.

Figure 5 shows the observed spectrum shape. The fit to a smooth curve has a poor chi squared, which improves if the mass window 70 GeV $< M_{\rm jetjet} <$ 100 GeV is excluded. The background subtracted peak is shown in Fig. 6. The expected contributions from W's and Z's are also shown. The total number of events in the peak is $N = 5618 \pm 1334$. The

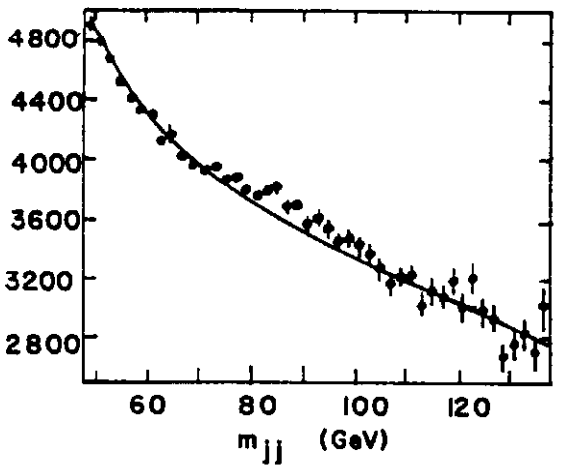

Figure 5: Jet-jet invariant mass distribution in the 50 to 130 GeV/c^2 mass region from UA2. The fit shown is to the QCD continuum background, with the mass window 70 GeV/c^2 $< m_{jj} <$ 100 GeV/c^2 omitted.

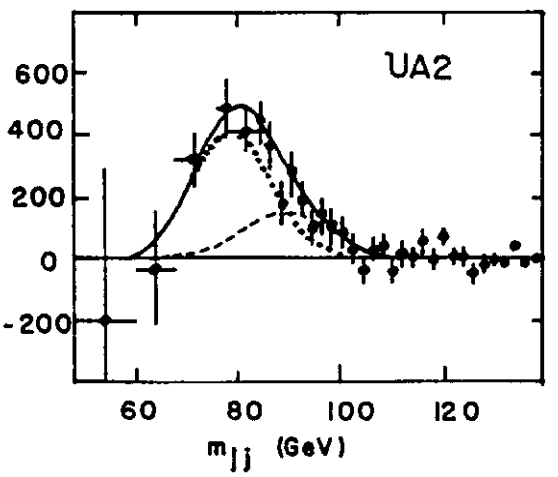

Figure 6: Data from Fig. 5 after subtraction of the QCD background. Expected relative sizes and shapes of the peaks from $W \rightarrow \bar{q}q$ and $Z \rightarrow \bar{q}q$ are shown.

expected number can be calculated from the standard model and the observed numbers of leptonic events $W \to e\nu$ and $Z \to e^+e^-$. Defining the ratio R, expected to be unity as:

$$R = \frac{N(W \to \text{jetjet})/\Gamma(W \to \text{jetjet}) + N(Z \to \text{jetjet})/\Gamma(Z \to \text{jetjet})}{N(W \to e\nu)/\Gamma(W \to e\nu) + N(Z \to e^+e^-)/\Gamma(Z \to e^+e^-)}$$
$$= 1.7 \pm 0.45. \quad (9)$$

Equation (9) does not allow for interference effects between gluon and W/Z jets [15]. The experimental yield is not sensitive to these effects at the present level of statistical accuracy.

Differences between quark and gluon jet patterns have been reported by the AMY group [16]. The gluon jets were broader and had lower leading particle rapidities than the quark jets. Other separation schemes based on fragmentation models have been considered by Jones [17] and Lonnblad *et al.* [18]. Since W and Z decay into quark jets, while the QCD background is dominated by gluons, experimental enhancement of the W/Z signal could be achieved by using such criteria, but there is no firm evidence from hadron colliders that these procedures are effective.

3 Electroweak Interactions

3.1 *Phenomenology*

There are several ways to define the parameters of the Electroweak Theory, all of which are equivalent in lowest order, but vary in their definitions when higher order radiative corrections are included. The magnitudes of these radiative corrections can be several percent. It is a tribute to the present accuracy of electroweak data that these corrections cannot be ignored. The convention of Marciano and Sirlin [19] will be adopted here, in which the Weinberg angle is defined in terms of the measured masses of the W and Z IVB's:

$$\sin^2\theta_W = 1 - \left(\frac{M_W}{M_Z}\right)^2. \quad (10)$$

The mass of the W is then related to the Fermi constant $G\mu$ by the formula:

$$M_W^2 = \frac{\pi\alpha}{\sqrt{2}G\mu}\frac{1}{\sin^2\theta_W}\frac{1}{(1-\Delta r)}, \quad (11)$$
$$= \frac{A}{\sin^2\theta_W(1-\Delta r)}, \quad (12)$$

where $1/\alpha = 137.0359895(61)$, and $G\mu = 1.16637(2) \times 10^{-5}$ GeV^{-2} [20]. $G\mu$ is derived from the muon decay rate and the muon mass after $O(\alpha)$ radiative corrections [21]. The constant

$$A = (37.2805 \pm 0.0003 \text{ GeV})^2. \quad (13)$$

Thus $A^{1/2}$, which is proportional to M_W, is known to one part in 10^5. The other precisely known quantity is M_Z [22]:

$$M_Z = 91.177 \pm 0.006 \pm 0.030 \text{ GeV/c}^2. \quad (14)$$

The 30 MeV/c^2 systematic error (3 parts in 10^4) comes from the calibration of the LEP ring energy, and may decrease in the future. The electroweak radiative correction term Δr in Eq. (12) is the link between the physics at the muon mass and at the W/Z mass, and may be written as the sum of several parts. Thus

$$\Delta r = \Delta\alpha - \cot^2\theta_W\Delta\rho + \ldots \quad (15)$$

The purely electromagnetic contribution $\Delta\alpha = 0.0601 \pm 0.0009$, while $\delta\rho$ depends quadratically on the top quark mass:

$$\Delta\rho = \frac{3\alpha}{4\pi\sin^2(2\theta_W)}\left(\frac{m_t}{M_Z}\right)^2; \quad (16)$$

and higher order terms include the logarithmic dependence on the mass of the Higgs boson [23]. Since neither m_t nor m_{Higgs} is known, there is some ambiguity in the interpretation of Δr once it is obtained from M_Z and M_W. Given Δr, as m_{Higgs} increases, so does m_t, but the variation in m_t is slow because m_{Higgs} only enters through $\log\left(\frac{m_{\text{Higgs}}}{M_Z}\right)$.

The parameter $\sin^2\theta_W$ appears in all neutral current weak interactions, and has been measured by the (neutral current)/(charged current) ratio in neutrino scattering [24]:

$$\sin^2\theta_W = 0.233 \pm 0.003 \pm 0.005. \quad (17)$$

Working entirely with the IVB masses avoids some ambiguity in the interpretation of the neutral current data and makes it clear precisely which scheme of radiative corrections is being used, so that the Weinberg angle defined in Eq. (10) will be retained throughout this discussion, although the results are in good agreement with Eq. (17).

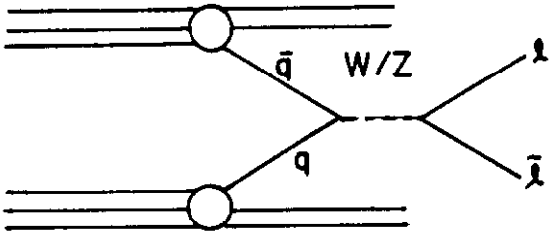

Figure 7: Parton model diagram for $\bar{p}+p \rightarrow W/Z + X$. A quark in the proton and an antiquark in the antiproton annihilate to form an on-shell IVB, which then decays into a lepton pair. The underlying event is formed by the qq and $\bar{q}\bar{q}$ noninteracting quarks. For Z production this diagram is analogous to and interferes with the Drell-Yan mechanism.

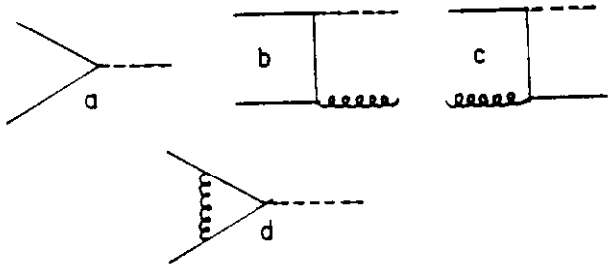

Figure 8: Diagrams which contribute to W/Z production with high IVB transverse momentum. These diagrams have no analog in the simple parton model.

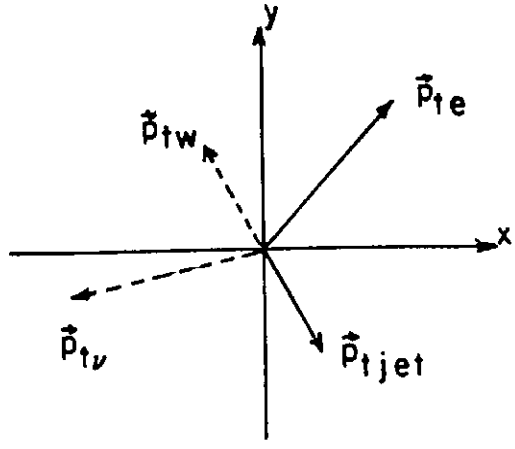

Figure 9: Vector diagram in the transverse plane showing the measured vectors $\vec{p}_{te}$ and $\vec{p}_{tjet}$, and the inferred vectors $\vec{p}_{tW} = -\vec{p}_{tjet}$, and $\vec{p}_{t\nu} = -\vec{p}_{te} - \vec{p}_{tjet}$.

The principal signatures used to detect the production and decay of W/Z intermediate bosons in $\bar{p}p$ collisions are the leptonic decays $W \rightarrow e\nu$, $W \rightarrow \mu\nu$, $Z \rightarrow e^+e^-$, and $Z \rightarrow \mu^+\mu^-$. The lowest order parton model diagram is shown in Fig. 7. This diagram is a reasonable approximation to W/Z production at 630 GeV, the energy of the CERN SPS collider, but the increase in jet activity at the 1.8 TeV Tevatron energy can only be explained by the higher order diagrams shown in Fig. 8. Jets which result in p_t distributions for W's and Z's have no analog in the simple parton model, and are therefore very important tests of QCD [25].

3.2 *W Mass*

The most important parameter of the EWK theory supplied by the hadron colliders is the mass of the W. Single $W^{\pm}$ production is possible because the $\bar{q}q$ collision can have a net charge even though the $\bar{p}p$ system does not. In the absence of a two body decay mode like $W^+ \rightarrow \pi + \gamma$ [26] or dramatic improvement in the jet-jet mass resolution described in Sec. 2 above, one is forced to work with $W \rightarrow e\nu$ and $W \rightarrow \mu\nu$. The longitudinal motion of both the W and the neutrino are unknown, and the mass reconstruction can be done only in the transverse plane. See Fig. 9. In this plane the transverse mass is de-

fined by:

$$M_T^2 = 2p_{te}p_{t\nu}\left(1 - \cos(\phi_{e\nu})\right). \qquad (18)$$

This is to be contrasted with the Breit-Wigner line shape for a completely constrained mass calculation:

$$\frac{dN}{dM} \cong \frac{s}{(s - M_W^2)^2 + (s\Gamma_W/M_W)^2} \qquad (19)$$

With perfect experimental resolution the distribution in M_T peaks at M_W, and has a high mass shape governed by Eq. (19). At lower masses there is a broad shoulder due to lepton p_t's less than $M_W/2$. In reality, the observed shape of the high mass edge is dominated by the resolution in the measurement of the p_t of the e or μ, and on the $p_{t\,\mathrm{jet}}$ resolution, from which the p_t of the neutrino is inferred:

$$\vec{p}_{t\nu} + \vec{p}_{te} = \vec{p}_{tW} = -\vec{p}_{t\,\mathrm{jet}}. \qquad (20)$$

Fluctuations in the measurement of the cylindrically symmetrical energy of the underlying event can also affect the $p_{t\nu}$ resolution. The shape of the M_T curve is not very sensitive to Γ_W, although there is a slight correlation between Γ and M_W, such that a given data set can be fitted to a lower mass with a broader width. The high mass edge is relatively insensitive to the longitudinal motion of the W, *i.e.*, to the choice of quark structure functions inside the p and $\bar{p}$. In the end, one must resort to monte carlo calculations as a function of M_W and Γ_W to fit the experimental distribution and extract a measurement of the W mass.

3.2.1 *UA2 Measurement*

The UA2 measurement of M_W was based on analysis of 1203 $W \to e\nu$ events in 7.1 pb^{-1} integrated luminosity at a center of mass energy of 630 GeV at the CERN SPS $\bar{p}p$ collider [27]. These events all had electrons in the central calorimeter fiducial volume, $|\eta| < 1.0$. The showers were well contained within the cells, *i.e.*, not near a cell boundary, and had $p_t > 20$ GeV/c. Candidates where the $p_{tW} > 20$ GeV/c were removed from the sample-about 5% of the data. This minimized the uncertainty in the calculation of $p_{t\nu}$ via Eq. (20) due to mismeasurement of hadronic energy. The p_t distributions of the electrons and neutrinos are shown in Fig. 10a and b, and

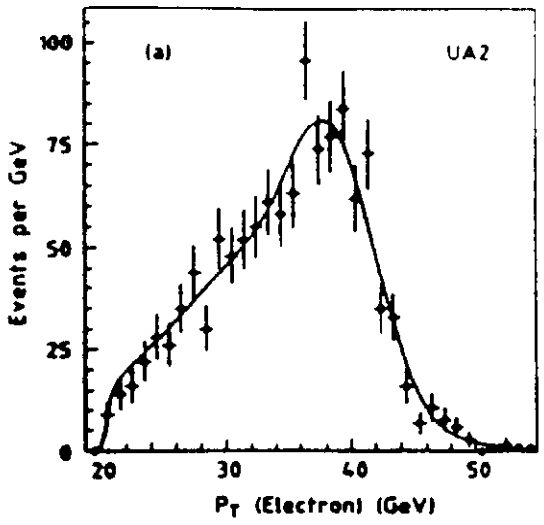

Figure 10a: p_{te} distribution for the UA2 data.

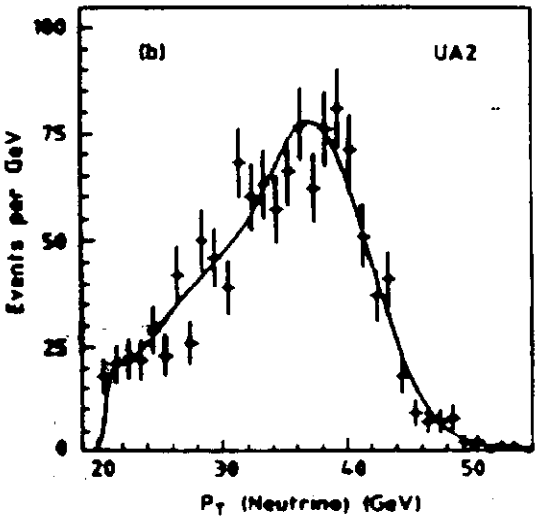

Figure 10b: $p_{t\nu}$ distribution for the UA2 data.

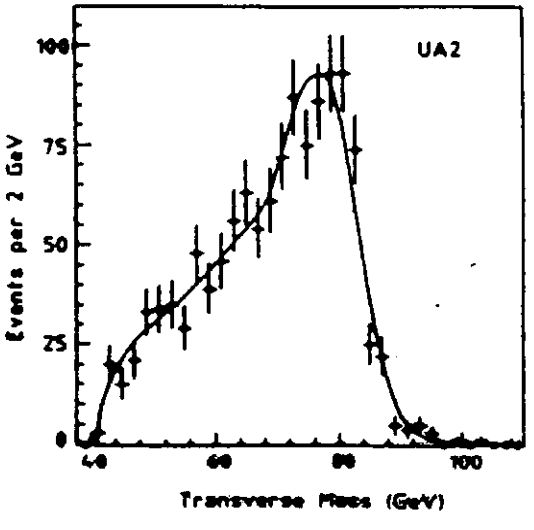

Figure 10c: M_T distribution calculated from Eq. (18) for the UA2 data. All figures come from Ref [27].

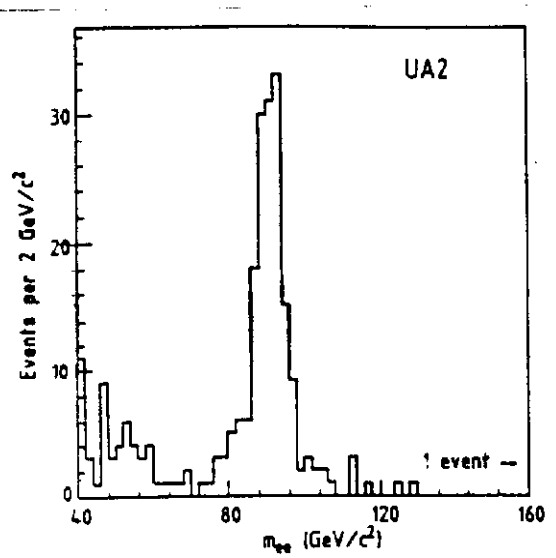

Figure 11: Invariant mass distribution of e^+e^- pairs in the Z peak region, from UA2.

the transverse mass calculated from Eq. (18) in Fig. 10c.

The energy scale was based on the response of the calorimeter cells to test beam electrons and had an uncertainty of 1%. In order to eliminate this uncertainty from the measurement of M_W, the UA2 group used a sample of electrons from $Z \rightarrow e^+e^-$ and the measurement of M_Z from LEP quoted in Eq. (14) above. The mass peak is shown in Fig. 11. This curve was fit to the Breit-Wigner form of Eq. (19) broadened by the experimental mass resolution and corrected for effects due to the underlying event, radiative Z decays, and the measurement of hadronic p_t. The final result is

$$M_Z = (91.49 \pm 0.35 \pm 0.12 \pm 0.92)\ \mathrm{GeV/c^2} \quad \text{(UA2)}, \qquad (21)$$
$$\text{stat} \quad \text{sys} \quad \text{scale}$$

where the 1% scale error is quoted separately from systematic uncertainties in the treatment of other effects.

The value of M_W was derived from fits to the distributions of Fig. 10 which were performed by the maximum likelihood method using expected shapes calculated by monte carlo. The M_T distribution gave the smallest errors, with the p_t distributions serving as a check on the correctness of the monte carlo model of the experimental data. See Ref. [27] for details. Consistent results for M_W were obtained with identical statistical errors whether the one parameter fit or the two parameter fit was used. The one parameter fit set $\Gamma_W = 2.1$ GeV/c^2, the standard model value assuming $m_t > M_W - m_b$, while in the two parameter fit Γ_W was allowed to vary. The monte carlo calculation of the M_T curve included experimental resolution effects due to electron energy measurement, the effect of p_{tW} on $p_{t\nu}$,and the parton structure functions. Uncertainties in the procedure contributed to the systematic error. The result is

$$M_W = (80.79 \pm 0.31 \pm 0.21 \pm 0.81)\ \mathrm{GeV/c^2} \quad \text{(UA2)}. \qquad (22)$$
$$\text{stat} \quad \text{sys} \quad \text{scale}$$

The scale error was eliminated by taking the ratio of Eq. (22) to Eq. (21):

$$\frac{M_W}{M_Z} = 0.8831 \pm 0.0048 \pm 0.0026 \quad \text{(UA2)}. \qquad (23)$$
$$\text{stat} \quad \text{sys}$$

Using Eq. (14) for M_Z then gives:

$$M_W = (80.50 \pm 0.43 \pm 0.24)\mathrm{GeV/c^2} \quad \text{(UA2)}. \qquad (24)$$
$$\text{stat} \quad \text{sys}$$

3.2.2 *CDF Measurement*

The CDF collaboration accumulated 4.7 pb^{-1} at 1.8 TeV in the $\bar{p}p$ center of mass. A complete description of the W mass analysis is presented in Ref. [28]. CDF employed basically the same procedure to extract M_W from $W \rightarrow e\nu$ as UA2. Indeed, the central EM calorimeters of the two experiments are quite similar. However, CDF analyzed $W \rightarrow \mu\nu$ decays as well, and had a smaller absolute scale error (.1% for muons and .2% for e's) because of the internal calibration using the solenoidal magnetic field and the known masses of the vector bosons J/ψ, ψ', and Υ. The higher center of mass energy meant that CDF enjoyed a cross section for W production about three times as large as UA2, but it also meant more jet activity, giving more transverse W motion, and more longitudinal W motion from the parton structure functions because of the smaller value of M_W^2/s.

Figure 12 shows the low mass calibration lines used to set the scale of the central tracking chamber momentum measurement. The peaks and the underlying Drell-Yan continuum come from momentum analysis of $\mu^+\mu^-$ pairs with $|\eta| < 1$. The positions of the peaks agree with the world average

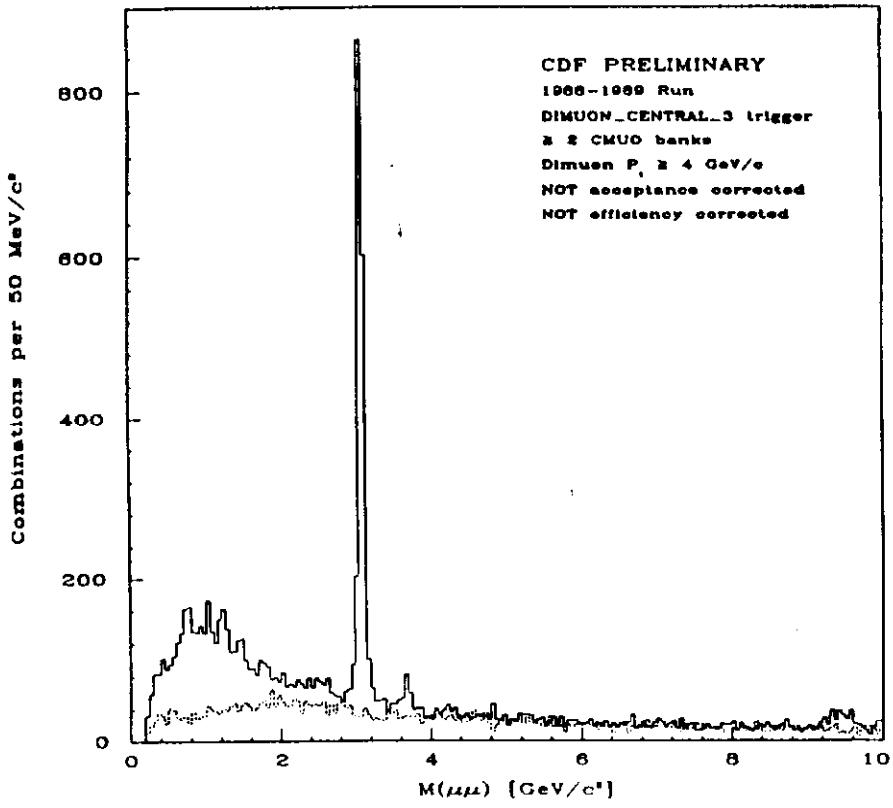

Figure 12a: CDF $\mu^+\mu^-$ spectrum in the low mass region, showing the prominent J/ψ peak. Like sign background is shown as a dotted line.

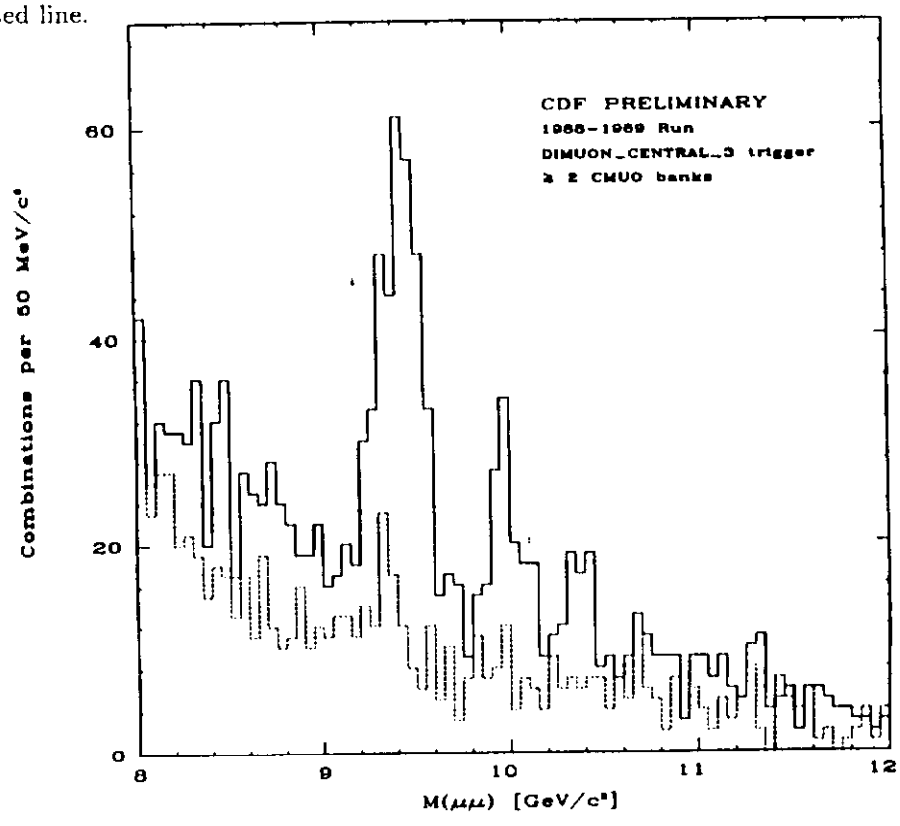

Figure 12b: Expanded view of the high mass region of 12a, showing the upsilon peaks.

values [20] to 0.1% without any adjustment of the detector constants—the magnetic field map and the tracking chamber wire positions. Hence the momentum scale averaged over + and − charge signs was known to this precision. Small charge dependent errors from incorrect azimuthal wire positions were corrected by using the calorimeter electromagnetic shower energies. Thus it was assumed that e^+ and e^- of the same energy gave the same signal in a given calorimeter tower. Differences in momentum measurement of such tracks were then eliminated by small shifts in the geometry. The W data sample was charge symmetric, so the sensitivity to these changes was small. The momentum resolution obtained after including the transverse beam position in the fit was $\Delta p_t/p_t = 0.0011$ pt (GeV), or about 1.3 GeV/c for the 35 GeV/c tracks typical of W decay leptons.

To transfer this absolute momentum scale to the calorimeter response, the towers were first normalized relative to each other. This was done using 17,000 inclusive electrons with $E_t > 15$ GeV—about 35 per calorimeter tower. Then W candidate electrons were used to set the energy scale absolutely by comparing E/p. W electrons were used because they came from a known source, so that radiative effects could be calculated, and the expected E/p distribution, assuming the absolute energy scale to be correct, could be predicted. The comparison of this prediction to the data is shown in Fig. 13. The final systematic uncertainty in the energy scale is 0.24%, compared to 0.1% for the momentum alone. The calorimeter energy resolution for electromagnetic showers measured in a test beam was

$$\left(\frac{\sigma_E}{E}\right)^2 = \left(\frac{13.5\%}{E_T}\right)^2 + (1.7\%)^2 \qquad (25)$$

where the constant term reflects the accuracy of the relative tower to tower normalization.

The resulting mass distributions for $\mu^+\mu^-$ and e^+e^- in the the Z mass region are shown in Fig. 14, taken from Ref. [29]. The weighted average result for M_Z quoted in Ref. [29] is:

$$M_Z = (90.9 \pm \underset{\text{stat+sys}}{0.3} \pm \underset{\text{scale}}{0.2}\ ) \text{ GeV/c}^2 \qquad (26)$$

in agreement with the more precise result in Eq. (14) above.

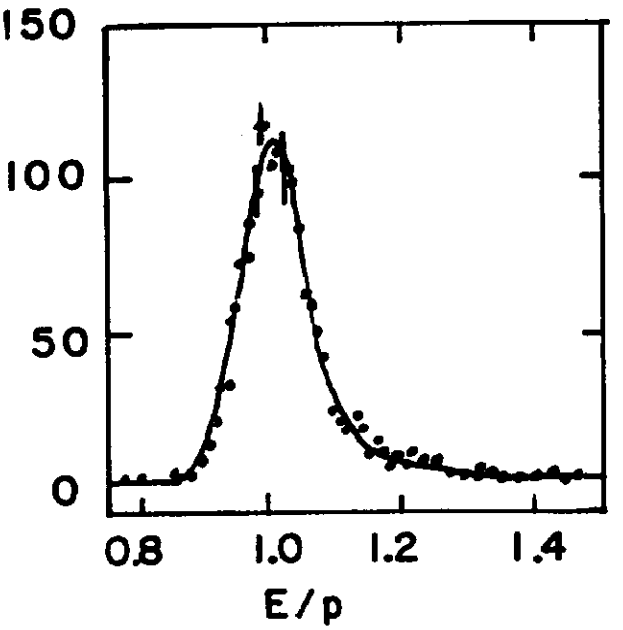

Figure 13: E/p comparison for CDF $W \rightarrow e$ electrons. The shape of the radiative tail calculated with the detector simulation program is compared to the data. $E/p > 1$ because the electron momentum is degraded by bremsstrahlung, but the resulting photons accompany the electron into the calorimeter.

Transverse mass distributions for $W \rightarrow e\nu$ and $W \rightarrow \mu\nu$ are shown in Fig. 15a and 15b respectively. The final data samples contained 1130 e's and 592 μ's after all cuts. The lepton $p_t > 25$ GeV was required, and e's were restricted to the same fiducial area used to calibrate the energy scale. To eliminate high p_t W's, events with a jet cluster above 7 GeV E_T were rejected. The useful integrated luminosity for the electron sample was 4.4 pb^{-1}, while for the muon sample it was 3.9 pb^{-1}. In addition, the acceptance of the central detector for e's was larger than for μ's. These two effects account for the factor of two difference in event yield.

The CDF fitting procedure involved a comparison between the observed and monte carlo predicted distributions as a function of (M_W, Γ_W) using the maximum likelihood technique in a manner similar to UA2. Both one parameter and two parameter fits were used. Predicted shapes for discreet values of (M_W, Γ_W) were interpolated to give continuous values of the unknown quantities. The final results quoted for Γ_W constrained to 2.1 GeV are:

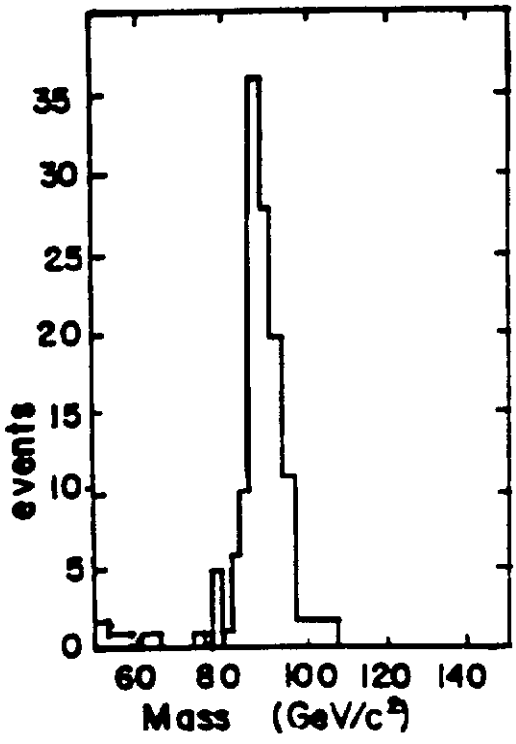

Figure 14a: CDF dimuon invariant mass spectrum in the region of the Z peak. The muon momenta were measured in the central tracking chamber.

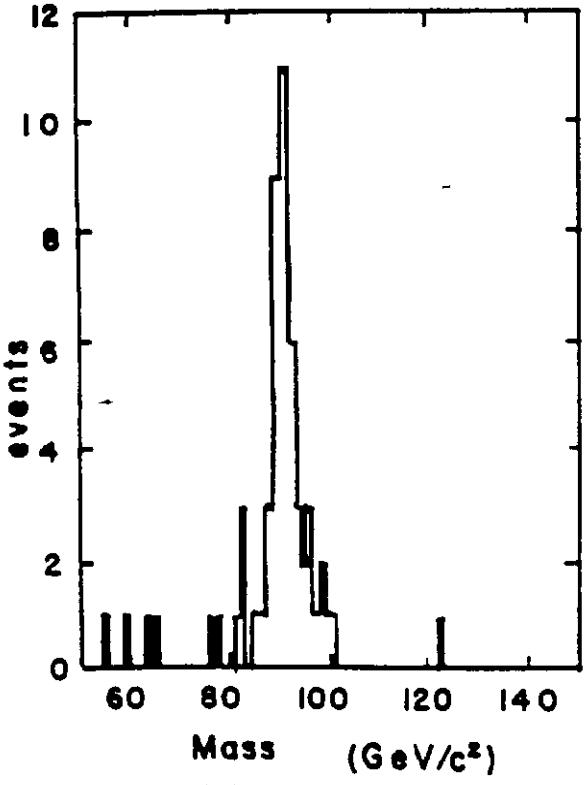

Figure 14b: CDF dielectron invariant mass spectrum measured with the calorimeters in the region of the Z peak.

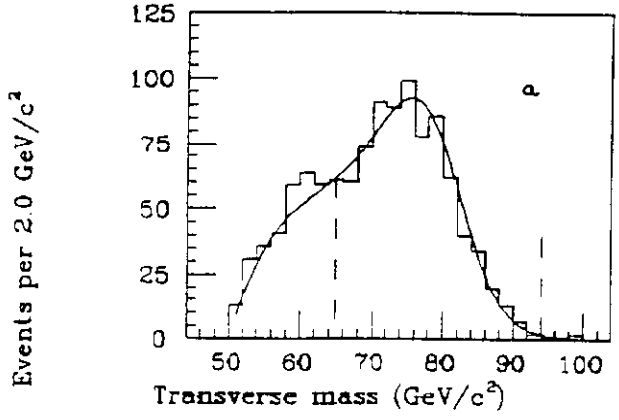

Figure 15a: CDF M_T plot for $W \to e\nu$.

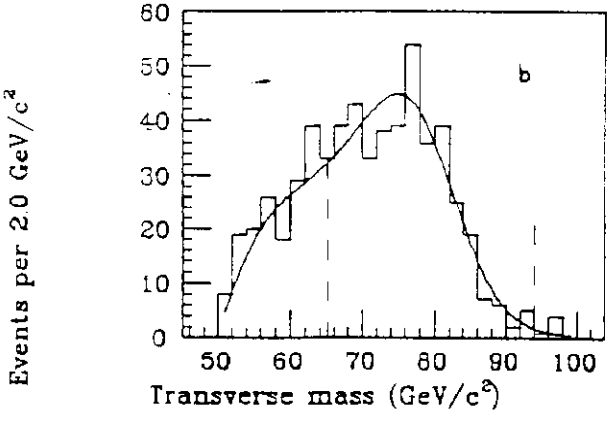

Figure 15b: CDF M_T plot for $W \to \mu\nu$.

$$M_W = (79.91 \pm 0.35 \pm 0.24 \pm 0.19)\ \mathrm{Gev/c^2}$$

(CDF e's)

$$M_W = (79.90 \pm 0.53 \pm 0.32 \pm 0.08)\ \mathrm{GeV/c^2}$$

stat sys scale

(CDF μ's)

(27)

Note that the scale errors are small compared to the statistical and other systematic errors, so there is no advantage to calculating the ratio $\frac{M_W}{M_Z}$ with present statistics. The systematic errors include uncertainties from the parton structure functions, the p_{tW} measurement, various possible backgrounds, and the fitting procedure. The two parameter fits are consistent with Eq. (27), but have slightly larger errors. The combined result, keeping track of common uncertainties in the two measurements, is

$$M_W = (79.91 \pm 0.39)\ \mathrm{GeV/c^2} \quad \text{(CDF)} \quad (28)$$

3.2.3 *Combined Results for M_W*

Equation (28) can be combined with Eq. (24) to give a best value of the W mass at the present time. To do this, a weighted average was calculated, combining the statistical and systematic errors of each measurement in quadrature. Since the techniques used to extract M_W were very similar, one might point out that the systematic errors for the two experiments are probably correlated, and this averaging technique may underestimate the final error. However, the statistical errors in each case dominate over the systematics, so the combined error cannot be too far off. The result is:

$$M_W = (80.15 \pm 0.31)\ \mathrm{GeV/c^2}\ \text{(UA2 and CDF combined)}. \quad (29)$$

3.3 *The Weinberg Angle and the Top Quark Mass*

The ratio $\frac{M_W}{M_Z}$ from Eq. (29) and Eq. (14) is

$$\frac{M_W}{M_Z} = 0.8791 \pm 0.0034, \quad (30)$$

which gives the Weinberg angle via Eq. (10) derived entirely from the IVB mass ratio:

$$\sin^2\theta_W = 0.2272 \pm 0.0060. \quad (31)$$

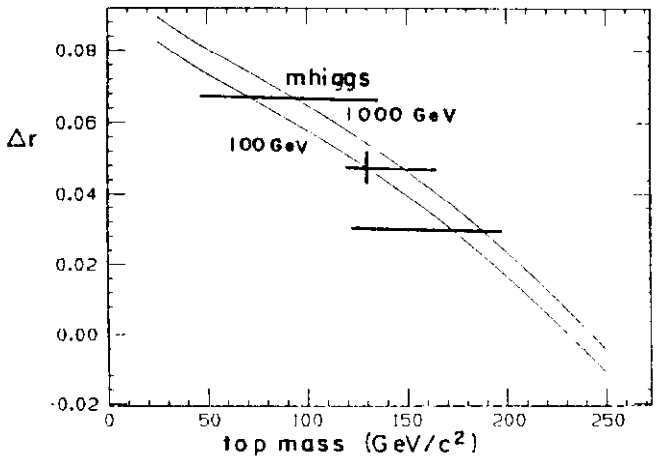

Figure 16: Δr defined by Eq. (11) calculated in Ref [30] as a function of m_{top} for $m_{\mathrm{Higgs}} = 100$ GeV and 1000 GeV.

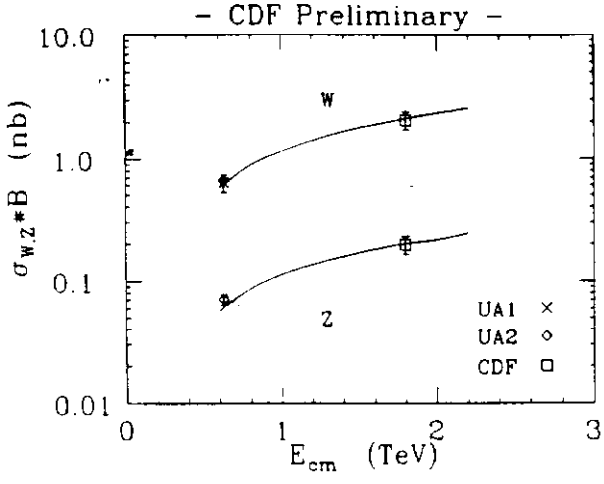

Figure 17: CDF individual cross section measurements for $\bar{p} + p \to W \to e\nu$ and $\bar{p} + p \to Z \to e^+e^-$ at 1.8 TeV compared to lower energy measurements at the SPS and theoretical expectations of Ref [34].

Then the radiative correction term Δr of Eq. (12) becomes:

$$\Delta r = 0.048 \pm 0.018 \qquad (32)$$

The top quark mass can then be read from Fig. 16 :

$$m_{\rm top} = 130^{+40}_{-60}\ {\rm GeV/c^2} \qquad ({\rm m_{Higgs}} = 100\ {\rm GeV/c^2}). \qquad (33)$$

If $m_{\rm Higgs} = 1000$ GeV/c^2, then the central value for $m_{\rm top}$ increases to 150 GeV/c^2. The curves for Δr vs $m_{\rm top}$ were derived from the formulas of Hollik [30] using the Z mass from Eq. (14) above.

3.4 *Cross Section Ratio and* Γ_W

It was pointed out when the first SPS collider results appeared in 1983 [31, 32] that the ratio

$$R = \frac{\sigma(\bar{p}p \to W) \cdot B(W \to e\nu)}{\sigma(\bar{p}p \to Z) \cdot B(Z \to e^+e^-)}, \qquad (34)$$

which is relatively free of experimental systematic errors, can be used to measure $\frac{\Gamma_Z}{\Gamma_W}$. The ratio can be rewritten as

$$R = \frac{\sigma(\bar{p}p \to W)}{\sigma(\bar{p}p \to Z)} \frac{\Gamma(W \to e\nu)}{\Gamma_W} \times \frac{\Gamma_Z}{\Gamma(Z \to e^+e^-)} \qquad (35)$$

In the Standard Model the leptonic partial width $\Gamma(W \to e\nu)$ can be expressed in terms of the W mass and the muon decay constant $G\mu$:

$$\Gamma(W \to e\nu) = \frac{G\mu M_W^3}{6\pi\sqrt{2}} \qquad (36)$$

This formula gives $\Gamma(W \to e\nu) = (0.225 \pm 0.003)$ GeV using Eq. (29). The Z leptonic width has been measured [22]: $\Gamma(Z \to e^+e^-) = (0.0837 \pm 0.0007)$ GeV. These numbers combine to $\Gamma(W \to e\nu)/\Gamma(Z \to e\epsilon) = 2.69 \pm 0.03$. Since $\Gamma_Z = (2.496 \pm 0.016)$ GeV [22], a formula can be obtained for Γ_W in terms of the cross section ratio:

$$\Gamma_W = \frac{\sigma(\bar{p}p \to Z)}{\sigma(\bar{p}p \to W)} \times R \times (6.71 \pm 0.08)\ {\rm GeV}. \qquad (37)$$

The cross section ratio has received much theoretical attention [33, 34]. Although many theoretical uncertainties cancel in the calculation, the ratio depends on the assumed parton distributions and on the QCD higher order diagrams to a degree which may cause concern, especially if the statistical error on the measurement of R decreases as more W/Z production data are accumulated at hadron colliders. Halzen and Keller [35] ascribe errors of 3% and 5% on the QCD-parton model calculations of $\frac{\sigma(W)}{\sigma(Z)}$ at 1800 GeV and 630 GeV respectively. Limited statistics in the number of Z's observed result in statistical errors in the measurements which are at present larger than these theoretical uncertainties.

Table 1: CROSS SECTION RATIO

EXP	R	# of Z	Γ_W
UA1	$10.08^{+1.14}_{-1.05}$	112	2.06 ± 0.23
UA2	$9.38^{+0.82}_{-0.72}$	169	$2.30 \pm 0.19 \pm 0.06$
CDF	$10.2 \pm 0.8 \pm 0.4$	187	2.19 ± 0.20

Table 1 summarizes the R measurements made by UA1 [36], UA2 [37], and CDF [38]. The experiments are in agreement with each other within the quoted errors. The average value of Γ_W is:

$$\Gamma_W = (2.17 \pm 0.12)\ {\rm GeV/c^2} \qquad ({\rm UA1,\ UA2,\ CDF}), \qquad (38)$$

which is in good agreement with 2.12 GeV/c^2 expected in the Standard Model. The individual cross sections were measured as well as the ratio, and these results are shown in Fig. 17.

3.5 *Charge Asymmetries in* $Z \to \ell^+\ell^-$ *and* $W \to \ell\nu$

Charge asymmetries due to γ-Z interference in e^+e^- annihilation below the Z peak have been extensively studied. The review by Marshall [39] covers the PEP and PETRA energy region, up to $\sqrt{s} = 40$ GeV, while the TRISTAN data are review by Kamae [40]. Final states $(\mu^+\mu^-)$, $(\tau^+\tau^-)$, and $(\bar{q}q)$ have all been studied. With the advent of LEP and SLC, these measurements have been extended to the Z resonance itself [22]. The cross section for $e^+e^- \to \bar{f}f$, where f is either a lepton or a light quark ($m_f^2/s \ll 1$), can be written [41]:

$$\frac{d\sigma}{d\Omega} = \frac{\alpha^2 \times N_c^f}{4s} \left(G_1(s)(1 + \cos^2\theta) + G_2(s) \times 2cos\theta \right), \qquad (39)$$

where θ is the angle between the incident e^- and the outgoing fermion. The forward-backward asymmetry $A_{FB} = \frac{\sigma_F - \sigma_B}{\sigma_F + \sigma_B}$ is the experimental quantity usually measured. The color factor $N_c^f = 1$ for leptons and 3 for quarks. The coefficient G_2 of the $\cos(\theta)$ term vanishes in the pure electromagnetic

limit, without the weak neutral current. The functions G_1 and G_2 are:

$$G_1(s) = Q_e^2 Q_f^2 + 2Q_e Q_f v_e v_f Re(\chi_o(s)) + (v_e^2 + a_e^2)(v_f^2 + a_f^2)|\chi_o(s)|^2$$

$$G_2(s) = 2Q_e Q_f a_e a_f Re(\chi_o(s)) + 4v_e a_e v_f a_f |\chi_o(s)|^2 \quad (40)$$

The first term in the $G_2(s)$ formula represents the interference between the vector photon and the axial vector component of the Z. The second term accounts for vector-axial vector interference at the Z peak. The Z propagator (normalized to the photon propagator) is

$$\chi_o(s) = \frac{s}{\sin^2(2\theta_W) \times (s - M_Z^2 + iM_Z\Gamma_Z)}. \quad (41)$$

The neutral current coupling constants used in Eq. (40) are given by:

$$v_f = I_3^f - 2Q_f \sin^2\theta_W$$
$$a_f = I_3^f \quad (42)$$

These definitions agree with the ones used by the Particle Data Group [20], and by Dydak [22]. The average values for the leptonic vector and axial vector couplings quoted in Ref. [22] are $v_\ell = -0.045 \pm 0.006$ and $a_\ell = -0.501 \pm 0.002$. The vector coupling is small because $\sin^2\theta_W$ is near 0.25. The charge asymmetry is therefore small on resonance, but the γ-Z interference can be large off resonance. The asymmetry also changes sign as the energy passes from below M_Z to above M_Z, giving a dramatic curve, shown in Fig. 18. This effect has been observed at LEP near the Z peak. For final state quarks the vector couplings are larger, resulting in somewhat larger asymmetries, albeit more difficult to measure experimentally.

Hadron colliders study the inverse reaction $\bar{q}q \to Z \to \ell^+\ell^-$. The formulas, being symmetric in initial and final fermion states, are the same. However, the initial state consists of distributions of quarks and antiquarks in the proton and antiproton, so the relative contributions of valence quarks and sea quarks become critical to the expected asymmetry [42]. Thus the sea × sea contribution is completely symmetric, while sea × valence or valence × valence will result in a correlation between the quark (proton) and the lepton (e^- or μ^-). Fortunately, the sea

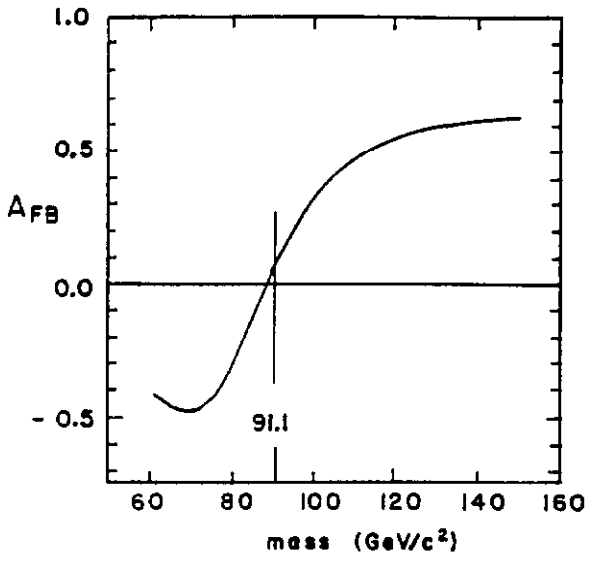

Figure 18: Charge asymmetry expected for $\bar{p} + p \to e^+e^-X$ in the mass region of the Z peak from Eq (39) and Ref [42]. Γ-Z interference, which changes sign at $s = M_Z^2$, can give large asymmetries just off resonance.

× sea contribution at 1.8 TeV is expected to be only about 20% of the total IVB production cross section, which slightly dilutes an already small asymmetry [33]. Further complication arises because the description above is given in the Z rest frame for collinear $q\bar{q}$ annihilation, a condition which does not hold at the Tevatron collider [43].

Preliminary results from CDF for the asymmetry in the decay $Z \to e^+e^-$ have been reported to this Conference by Franklin [44]. The angular distribution for 252 events with 75 GeV $< Mee <$ 105 GeV is shown in Fig. 19. The results are:

$$A_{FB} = (5.2 \pm \underset{\text{stat}}{5.9} \pm \underset{\text{sys}}{0.4})\% \quad \text{CDF Preliminary}$$
$$\sin^2\theta_W = 0.228 \pm \underset{\text{stat}}{0.016} \pm \underset{\text{sys}}{0.002}. \quad (43)$$

The lepton asymmetry for $q\bar{q} \to W^- \to e^-\nu$ can be treated from a different perspective, since in this case the angular distribution of e^- in the W^- rest frame has the form $(1 + \cos\theta)^2$, where θ is the angle between the e^- and the incident quark (consistent with Eq. (39)). This distribution is a consequence of the V-A character of the charged weak current. Thus the lepton asymmetry from polarized W's is a basic component of the theory, with no free parameters. In addition this asymmetry has been confirmed

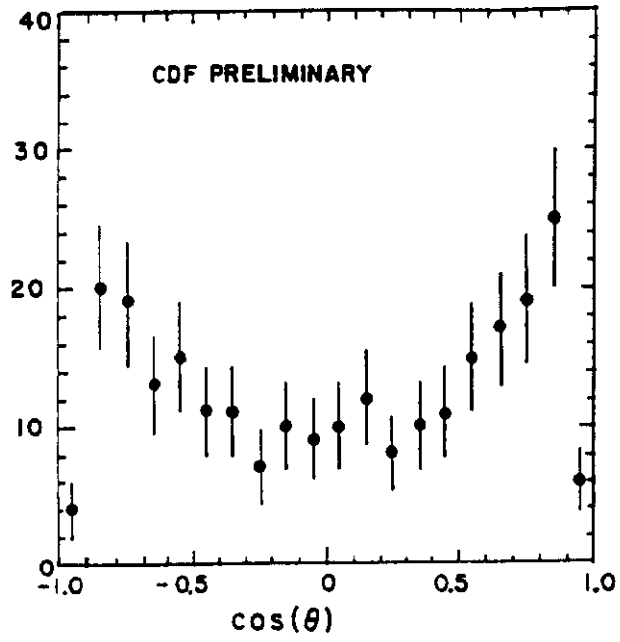

Figure 19: Preliminary CDF data for the $Z \rightarrow e^+e^-$ charge asymmetry. The sign convention is consistent with Eq (39).

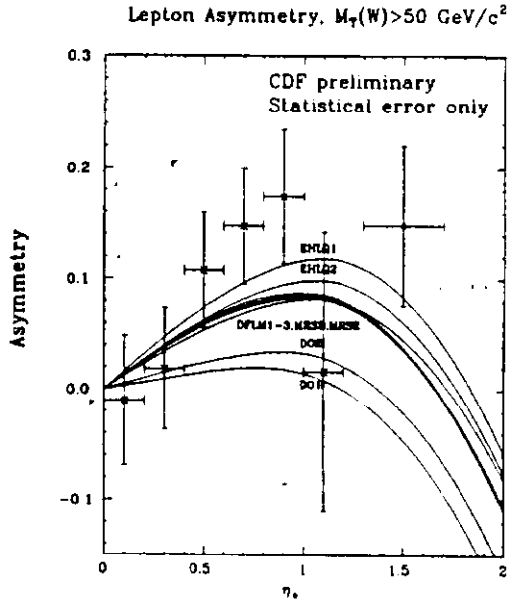

Figure 20: Preliminary CDF data for the $W \rightarrow e$ charge asymmetry in the central rapidity region. The asymmetry at a particular value of eta is defined as: $A(\eta) = (Ne+(\eta > 0)+Ne-(\eta < 0)-Ne+(\eta < 0)-Ne-(\eta > 0))/\text{sum}$. This convention is opposite to the one in Fig. 18. On resonance, the signs of the $q \rightarrow e^-$ asymmetries in the W^- and Z rest frames are the same.

by experiment at the SPS [36]. At the Tevatron the broad distribution in W rapidity together with the kinematic ambiguity due to the zero constraint fit preclude the Lorentz transformation of the lepton into the W rest frame except at very small angles relative to the colliding beams. Thus in the central region of rapidity one must be content with the measurement of the asymmetry in the lepton rapidity distribution in the laboratory frame, which is a convolution of the lepton rapidity distribution in the W rest frame and the W rapidity distribution in the laboratory.

These two rapidity distributions have opposite signs. The helicity rules require the e^- from W^- decay to favor the initial d quark direction, or (predominantly) the proton direction. Hence the weak interaction prefers a reversal of the flow of charge. The valence quark structure functions on the other hand favor the production of W^- along the antiproton direction, since $u(x)$, the u quark structure function, falls off more slowly with increasing x than does $d(x)$. W production tends to preserve the flow of charge. Fig. 20 shows preliminary results from CDF for $W \rightarrow e\nu$ lepton asymmetry in the central region, compared to the predictions of several struc-

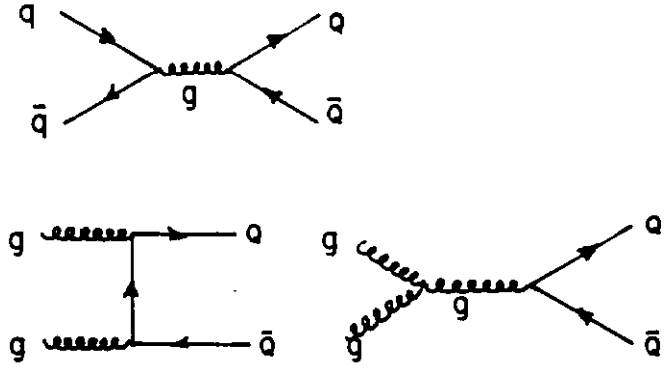

Figure 21: QCD diagrams for the production of heavy quarks by light quarks and gluons.

ture functions. Note that the asymmetry is positive, which is opposite to that expected from the helicity rules, so that in the central region the W motion predominates. Such measurements can contribute valuable information to the process of fitting the structure functions, and in turn improve the accuracy of the prediction of the cross section ratio Eq. (34). See Ref. [35].

4 Heavy Flavor Lost and Found

4.1 *Bottom Quarks Found*

Mesons containing the fifth quark, the b with charge $-1/3$, have been extensively studied at e^+e^- colliders [39, 40] since the discovery of the Υ (4S) at CESR in 1980 [45]. Almost everything known about B decays comes from e^+e^- colliders: CESR and DORIS running at the upsilon (4S) "B factory", and PEP and PETRA running at higher energy. These studies include measurement of the leptonic branching ratios, exclusive final states like $B \to J/\psi K^*$ and the B mass, $(b \to u)/(b \to c)$ via the lepton spectrum, the B lifetime, and B-$\bar{B}$ mixing [46].

Hadron colliders offer the possibility of high statistics detailed studies of B decays because of the large ($> 10\ \mu b$) cross section for $\bar{p}p \to \bar{b}b + X$ at collider energies. The dominant diagram is gluon-gluon fusion—see Fig. 21. An integrated luminosity of 10 pb^{-1} would produce 10^8 events. The experimental challenge is to detect a reasonable fraction of them by tagging the B through its decay channels or its finite flight path or both, in the presence of very large light quark and gluon backgrounds, and thus to exploit this rich physics potential.

The UA1 collaboration led the way in demonstrating that hadron colliders might one day serve as their own brand of B factories [47, 48]. The signature used by UA1 was muon pairs arising from heavy flavor semileptonic decays:

$$\begin{array}{ccccc} \bar{p} + p \to & \bar{b} & + b & + X & \qquad (44) \\ & \hookrightarrow \bar{c}\mu^+\nu & \hookrightarrow c\mu^-\nu & & \end{array}$$

A cut on the muon $p_t > 3$ GeV/c favored the heavy quark decay, as did the dimuon mass $m_{\mu\mu} > 6$ GeV/c. Some muons from the decay of the $\bar{c}$ or c quark either in the flavor cascade or from direct production of $\bar{c}c$ pairs were included in the sample, as were background muons from π and K decay in flight. Decay in flight was studied by using the single high p_t muon inclusive sample, and selecting events where there was a second high p_t charged track. Muon decay of the second track was then simulated by monte carlo. By fitting the spectrum of muon pt relative to the jet axis for nonisolated events, a signal of $66 \pm 10\%$ muons from $\bar{b}b$ was obtained.

Muon pairs from $\bar{b}b$ decay have unlike signs, except if $\bar{B}$ and B mix. The possibility exists for B° and $\bar{B}^\circ$ to mix in analogy with the $\bar{K}K$ system. The transitions $(\bar{b}d) \to (\bar{d}b)$ or $(\bar{b}s) \to (\bar{s}b)$ are second order in the weak interaction. The Cabibbo-Kobayashi-Maskawa (CKM) [49] matrix elements should favor the $(\bar{b}s)$ mixing case, but there is so far no unambiguous experimental evidence that B_s mesons mix, although mixing for B_d is now well established [50].

UA1 reported to this conference [51] an update on their earlier measurement [48] of $\bar{B}B$ mixing using unlike sign vs like sign dimuons. The mixing parameter is defined by UA1 as

$$\chi = \frac{N(B^\circ \to \bar{B}^\circ \to \mu^+\nu X)}{N(B^\circ \to \mu^-\nu X) + N(B^\circ \to \bar{B}^\circ \to \mu^+\nu X)}. \qquad (45)$$

The e^+e^- groups use the quantity r which omits the mixed term in the denominator. The basic measurement by UA1 was straightforward: compare the number of like sign and unlike sign muon pairs where each muon $p_t > 3$ GeV/c. Substantial complications arise in extracting χ from this uncorrected number, because there are sources of muon pairs other than B decay; there are B^+B^- which cannot mix as well as $B^\circ\bar{B}^\circ$ which can; and there are B_s° and B_d° neutrals. The UA1 preliminary result from the new data after all corrections is:

$$\chi = 0.16 \pm 0.06 \pm 0.02 \qquad \text{(UA1 Preliminary)}, \quad (46)$$

which is in good agreement with Ref. [52]. Figure 22 shows a plot of the UA1 result, which cannot distinguish between B_d and B_s mixing, compared to the e^+e^- result from running at the upsilon (4S) which is unambiguously B_d mixing.

The difference ΔM between the mass eigenstates of the B° system, and in turn the mixing parame-

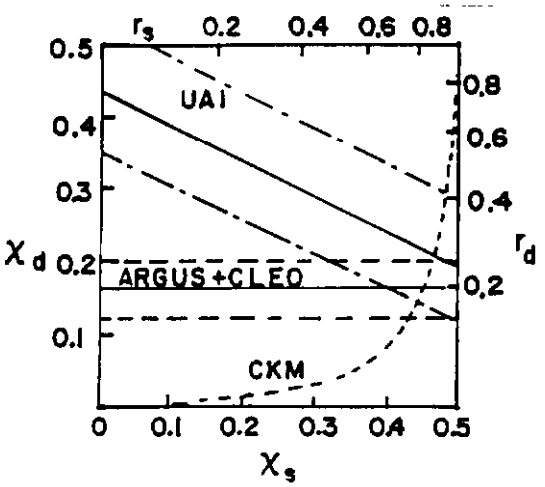

Figure 22: A comparison of the mixing parameter results of UA1, CLEO, and ARGUS, taken from Ref [51]. The UA1 data were interpreted assuming that a fraction 0.36 of all b quarks form B_d°, and 0.18 form B_s°. The one sigma error bars are shown on the UA1 data. The CKM curve favors $\chi_s > \chi_d$.

ter r depend on the top quark mass. It therefore is possible to calculate $m_{\rm top}$ using elements of the CKM matrix [53]. One complication of this approach is that, because the mixing involves mesons rather than quarks, a bag model parameter B_B enters the formula for r. It is possible however to obtain a prediction for $m_{\rm top}$ consistent with Eq. (33) using a reasonable value for B_B. This is interesting because it is completely independent of the electroweak radiative correction arguments and of the mass of the Higgs.

UA1 and CDF have both searched for the rare decay $B^\circ \to \mu^+\mu^-$. The branching ratio for this decay in the Standard Model is expected to be about 5×10^{-10} for $m_{\rm top} = 100$ GeV [54]. The decay is a flavor changing neutral current, and hence must proceed via the exchange of two W bosons, or a W and a Z. The analogous decay $Br(K_L^\circ \to \mu^+\mu^-) = (6.3 \pm 1.1) \times 10^{-9}$ [20]. In an extension of the Standard Model to include charged scalar fields the branching ratio could increase to the 10^{-8} to 10^{-9} range [54]. Either case is out of range of present experiments.

UA1 has also searched for the inclusive channel $B^\circ \to \mu^+\mu^- X$. In this case the J/ψ resonance formation and subsequent decay into muon pairs has been observed, but not the nonresonant continuum. The continuum branching ratio in the Standard Model could be in the 10^{-5} to 10^{-6} range [55], which is approaching experimental accessibility.

Table 2: Rare decays

	UA1	CDF	Standard Model
$B^\circ \to \mu^+\mu^-$	$< 8 \times 10^{-6}$	$< 3 \times 10^{-6}$	10^{-8} to 10^{-9}
$B^\circ \to \mu^+\mu^- X$	$< 5 \times 10^{-5}$	—	10^{-5} to 10^{-6}

90% confidence

Table 3: Relative J/ψ Yield

Source	direct	χ_0	χ_1	χ_2	B	ψ'
relative yield	0.05	0.005	0.44	0.14	1.0	0.002

The search involved making a dimuon invariant mass plot, and looking for a peak in the range 5.1 GeV/c^2 $< m_{\mu\mu} <$ 5.5 GeV/c^2 for $B^\circ \to \mu^+\mu^-$, and an excess above the Drell-Yan continuum between 3.9 GeV/c^2 and 4.5 GeV/c^2 for the inclusive channel. No evidence of a signal was observed, resulting in the limits summarized in Table 2.

CDF has reported to this Conference the successful use of the decay $J/\psi \to \mu^+\mu^-$ as a tag for B decays [56]. Figure 23 shows the dimuon data from Fig. 12 in the J/ψ and ψ' mass regions. There are 1500 J/ψ's and 72 ± 17 ψ''s above background in these plots, based on an integrated luminosity of 4 pb^{-1}. The p_t distribution is shown in Fig. 24. The trigger placed an effective threshold $p_t > 5$ GeV/c on the muon pair, and the data were restricted to the central region $|\eta| < 0.5$. At hadron collider energies, where the $\bar{b}b$ production cross section is large, B decays furnish a substantial fraction of all J/ψ's produced [57]. There are four sources of J/ψ's:

a.) direct production, $\bar{p}p \to J/\psi + X$;

b.) $\bar{p}p \to \chi \to J/\psi + \gamma$;

c.) $\bar{p}p \to B \to J/\psi + X$; and

d.) $\bar{p}p \to \psi' \to J/\psi\pi^+\pi^-$.

The calculated relative rates for $J/\psi \to \mu^+\mu^-$ from these various sources at 1.8 TeV with $p_t > 5$ GeV/c are given in Table 3. About 2/3 of all J/ψ's come from B's, with most of the remainder coming from

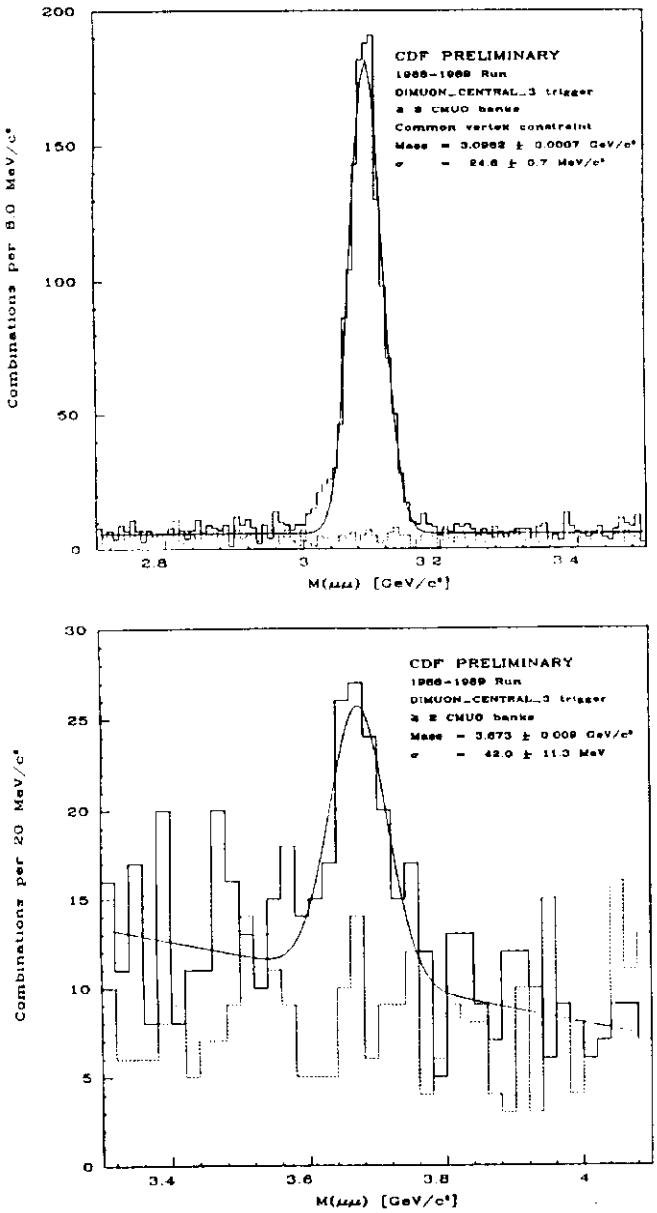

Figure 23: CDF J/ψ and ψ' peaks from Fig. 12.

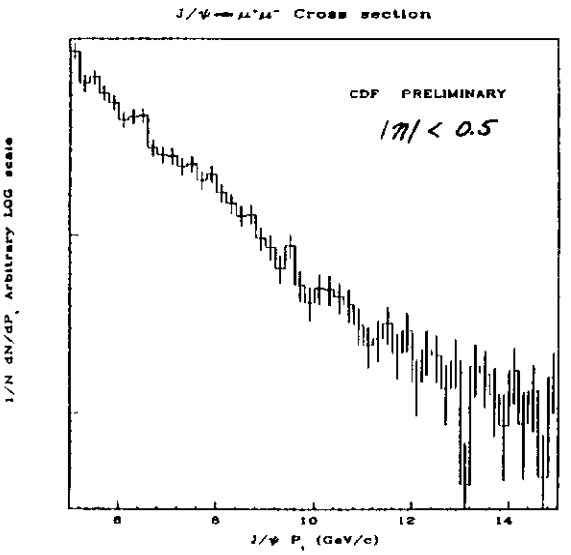

Figure 24: CDF preliminary J/ψ p_t distribution.

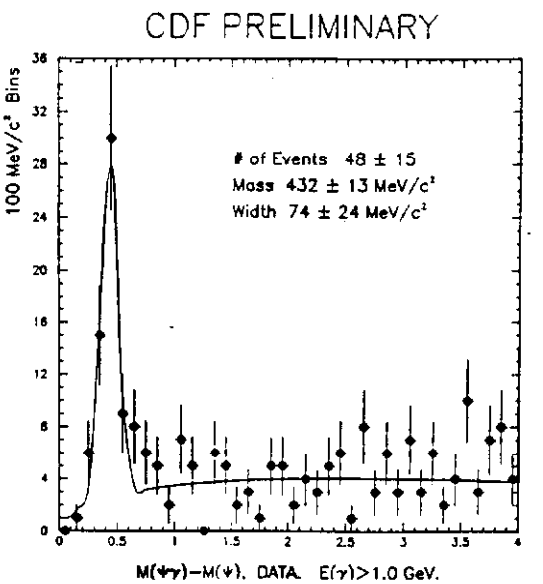

Figure 25: CDF preliminary invariant mass plot for $J/\psi + \gamma$, showing the low mass peak consistent with expectations from $\chi \to J/\psi + \gamma$.

the χ state with $J^{PC} = 1^{++}$. The 0^{++} state is suppressed both by a small production cross section and a lower branching ratio $Br(\chi_0 \to J/\psi + \gamma) = 0.7\%$. Direct production and daughters of ψ' decay can be neglected. So only two of the χ states contribute to $J/\psi + \gamma$, and χ's and B's dominate the high p_t J/ψ signal.

The branching ratio for $B \to J/\psi + X = (1.12 \pm 0.18)\%$ of all B decays—either charged or neutral, while $B \to \psi' + X = (0.46 \pm 0.17)\%$ [20]. Since the χ states are energetically forbidden from decaying into ψ', and direct ψ' production is expected to be small, $B \to \psi' + X$ may be assumed the only source of ψ'. The ratio of observed J/ψ to ψ' in the data can thus be used to calculate the fraction of J/ψ's which come from B decay. The results are:

$$\psi'/(J/\psi) = (4.3 \pm 1.0)\% \qquad \text{CDF Preliminary,} \tag{47}$$

to be compared with the upsilon (4S) result [58]:

$$\psi'/(J/\psi) = (6.8 \pm 2.5)\% \qquad \text{CLEO.} \tag{48}$$

The ratio of these two numbers, assuming all of the CLEO events came from B decays, is the fraction of J/ψ from B decay:

$$F = 64\% \pm 15\%_{\text{stat}} \pm 5\%_{\text{syst}} \pm 23\%_{\text{stat}} \qquad \text{CDF Preliminary,} \tag{49}$$

where the second statistical error is from Eq. (48). This large fraction, in agreement with expectations, indicates that the J/ψ tag can be efficiently exploited to identify B meson production in the presence of backgrounds.

CDF also reported observation of several exclusive decay channels using the $J/\psi \to \mu^+\mu^-$ tag. An independent check of the assumption that the remaining 36% of the J/ψ's came from χ decay was obtained by searching for gamma ray conversions in the central detector with $E_\gamma > 1$ GeV , and reconstructing the $J/\psi\gamma$ invariant mass. Figure 25 shows the resulting spectrum after applying an isolation cut to the photon to suppress background from B's. The position of the peak is consistent with the expected mixture of 1^{++} and 2^{++} χ's. After correction for the χ detection efficiency calculated by monte carlo, the yield of 48 ± 15 events in the peak agrees with the hypothesis that all J/ψ's came either from B or χ decay.

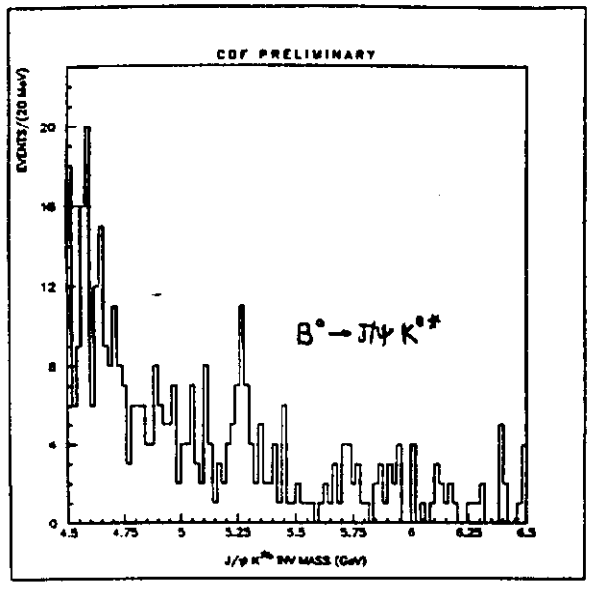

Figure 26: CDF preliminary invariant mass plot for $J/\psi + K^{*o}$. To make this plot pairs of ($\pm$) charged tracks were assigned (π, K) or (K, π) masses and the invariant mass of the (J/ψ, π, K) was calculated for those (π, K) combinations within $\pm$50 MeV of the K^* mass (896 MeV).

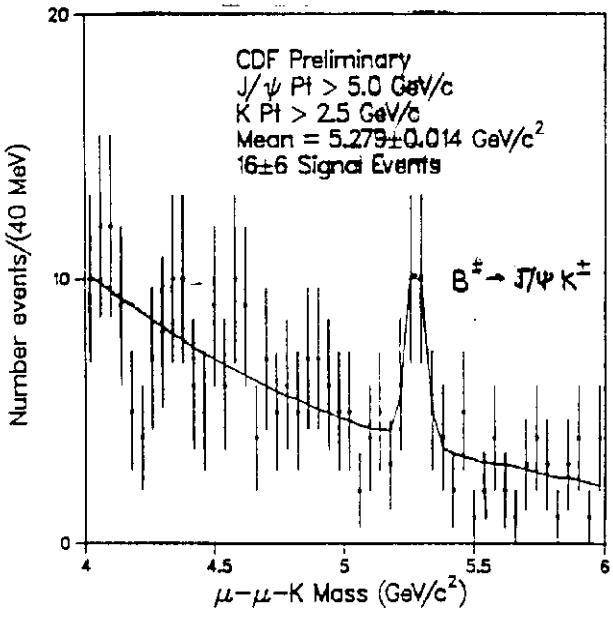

Figure 27: CDF preliminary invariant mass plot for $J/\psi K^{\pm}$. To make this plot all charged particles in a 60 degree cone about the J/ψ direction above 3 GeV pt were assigned the K mass, and the invariant (J/ψ, K) mass was calculated.

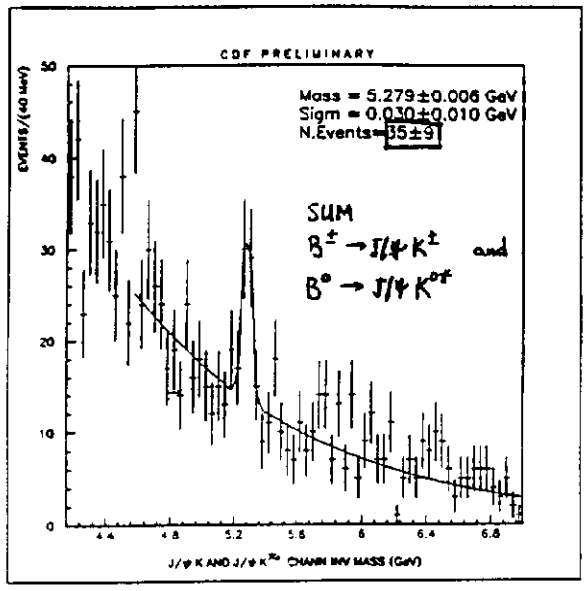

Figure 28: Combined data from Figs 26 and 27.

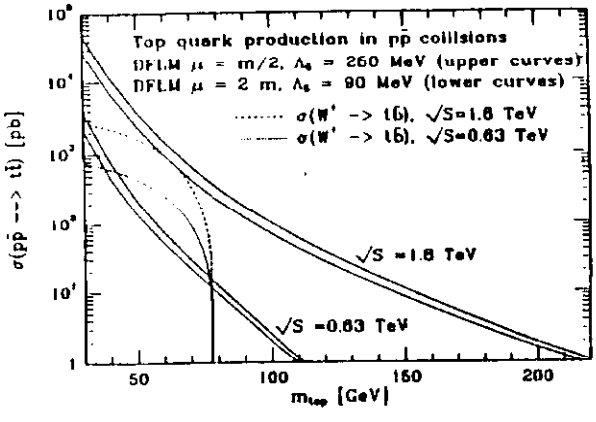

Figure 29: Cross section for $\bar{p} + p \to$ top quark as a function of $m_{\rm top}$, from Ref. [60]. At SPS energies the sensitivity is largest for $m_{\rm top} < M_W - m_b$, where $\bar{p} + p \to W \to t\bar{b}$ is the dominant source of top. At the Tevatron direct pair production $\bar{p}p \to \bar{t}tX$ dominates for all $m_{\rm top}$.

Searches for exclusive B decays in the $J/\psi \to \mu^+\mu^-$ data sample have also born fruit. Figure 26 shows the invariant mass plot sensitive to $B^0 \to J/\psi + K^{0*}$, $K^{0*} \to K^+\pi^-$. The K^{0*} was reconstructed by picking each charged track in the J/ψ event, searching for another charged track of the opposite sign in a 60° cone, and then assuming the (K, π) and (π, K) mass assignments. CDF had no instrument for distinguishing π's and K's, and the J/ψ did not indicate whether the parent meson was a B or a $\bar{B}$. The considerable combinatorial background is shown in Fig. 26, together with a peak at 5.28 GeV consistent with the B mass. A similar procedure was used to look for the two body decay $B^{\pm} \to J/\psi K^{\pm}$, shown in Fig. 27. Figure 28 shows the two plots combined. These preliminary data confirm the utility of the J/ψ tag as a signature for B production at hadron colliders.

4.2 *Top Quarks Lost*

4.2.1 *Introduction*

If not really lost, the top quark is not exactly found either. The search for the charge +2/3 top quark has a long history, dating back to the discovery of its companion, the bottom [59]. Early work concentrated on a change in the ratio $R = (e^+e^- \to \text{hadrons})/(e^+e^- \to \mu^+\mu^-)$ which would either indicate the presence of a toponium peak or an increase in R by 4/3 (which becomes 1.07 after QCD corrections) at the threshold for the production of a new quark pair. The absence of any change in R at PETRA energies implied a limit $m_{\rm top} > 23.3$ GeV/c^2 [39]. This technique was extended at TRISTAN to $m_{\rm top} > 28$ GeV/c^2 by the same technique [40]. LEP and SLC have extended the limit to $m_{\rm top} > 46$ GeV/c^2 by searching for $e^+e^- \to t\bar{t}$ with $t \to bW^*$ where W^* is an off shell W [22].

A key ingredient in determining the sensitivity of a hadron collider search is the cross section for the production of the top in $\bar{p}p$ collisions. This is shown as a function of the top quark mass in Fig. 29. At $\sqrt{s} = 630$ GeV, the dominant source of top quarks is $W^+ \to t\bar{b}$ [60], provided of course that $m_{\rm top} < M_W - m_b$. For a heavier top the cross section is < 10 pb. Every top quark search at hadron colliders, with

perhaps one or two exceptions*, has been based on the Standard Model decay chain:

$$t \to b + W^*;\ W^* \to \underset{11\%}{e\nu}\ ,\ \underset{11\%}{\mu\nu}\ ,\ \underset{11\%}{\tau\nu}\ ,\ \underset{67\%}{q\bar{q}}\ , \quad (50)$$

where the asterisk signifies an off-shell W if $m_{\rm top} < M_W + m_b$, and the branching fractions of the final states are written below. In order to suppress QCD jet background, a high p_t lepton, either e or μ, is required. At the SPS the top quark events would have the form:

$$\begin{array}{l} \bar{p}p \to W^+ \qquad X \qquad (51) \\ \quad \llcorner\ t\bar{b} \\ \quad\quad \llcorner\ bW^{*+} \\ \quad\quad\quad \llcorner\ \mu^+\nu. \end{array}$$

In this example there would be a high p_t μ^+ and jet activity associated with the fragmentation of the b quarks. There would also be a large missing E_T from the neutrino accompanying the W^* decay.

4.2.2 *Searches at the SPS*

The first hadron collider search for the top quark was made by the UA1 group at the SPS [61]. The inclusive muon pt spectrum after background subtraction was consistent with (c,b) quark decays, Drell-Yan, J/ψ, and Υ muon pairs, and W and Z decays. In the muon sample where $p_t\mu > 10$ GeV/c and $E_{Tjet} > 10$ Gev, the distribution of muon p_t relative to the jet axis was well described by $\bar{c}c + \bar{b}b$ decays together with a small background from π and K decay. To enhance the possible top signal, an isolation requirement was made on the muon, at least one jet with $E_T > 12$ GeV was required, and the transverse mass $M_T(\mu\nu) < 40$ GeV. The M_T requirement eliminated W events from the sample. The resulting conservative limit, based on no departure of the data from expectations without the top quark, was $m_{\rm top} > 44$ GeV/c^2.

Both UA1 and UA2 reported to this conference the latest limits on the top quark mass based on their most recent data [62, 63]. Combining the new muon data with the earlier sample, UA1 by a similar analysis to the one described above obtained a new limit $m_{\rm top} > 52$ GeV/c^2 (95%cl).

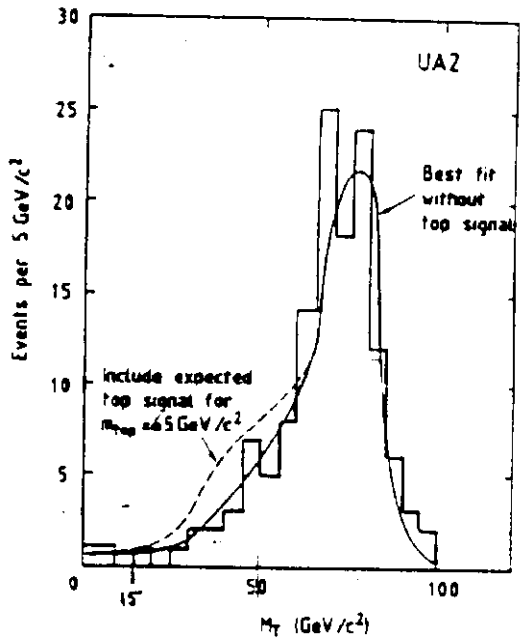

Figure 30: UA2 W+ jets transverse mass plot to look for top. The dotted curve shows the signal expected from a 65 GeV/c^2 top.

UA2 worked with high p_t electrons, and plotted the transverse mass for electron events with $p_te > 12$ GeV/c and at least one jet with $E_T > 10$ GeV. The transverse mass was calculated via Eq. (18), and the resulting plot, shown in Fig. 30, resembles the one in Fig. 10c, but has only 137 events because of the jet E_T requirement. The limit on top quark production was based on the observation that if 40 GeV/c^2 $< m_{\rm top} <$ 70 GeV/c^2, then the decay of the W^* from $t \to W^*b$ would reconstruct as a low mass W on the M_T plot, and hence give an enhanced signal below the real W peak. The dashed curve in Fig. 30 shows the expected enhancement for a 65 GeV/c^2 top. The UA2 result was

$$m_{\rm top} > 71 \text{ GeV/c}^2 \quad (90\% \text{ confidence}) \text{ (UA2)}. \quad (52)$$

Figure 29 shows that the expected cross section at the Tevatron, $\sqrt{s} = 1.8$ TeV, is dominated by $\bar{p}p \to \bar{t}t + X$ for all values of $m_{\rm top}$, and the cross section is 100 pb for $m_{\rm top} = 100$ GeV. Thus the higher energy gives an enhanced reach in the top quark search, but at the price of greater theoretical uncertainty in the cross section, since the $W \to t\bar{b}$ channel can be predicted given the rate for $W \to$

*UA1, for example, has searched for $t \to H^+b$, where H^+ is a charged scalar. See Ref. [36].

$e\nu$. Much theoretical effort has been applied to the question of heavy quark pair production, and it is estimated that the uncertainty in the cross section calculation for a heavy top is in the 10% to 20% range [60].

4.2.3 *Searches at the Tevatron*

Events at the Tevatron have the following topology:

$$\begin{array}{ccccc} \bar{p}+p \rightarrow & \bar{t} & & +t & +X \\ & \hookrightarrow \bar{b}W^{-*} & & \hookrightarrow bW^{+*} & \\ & \hookrightarrow \mu^-\nu & & \hookrightarrow \bar{q}q & \end{array} \qquad (53)$$

The event in this example would have a high p_t isolated μ^-, two energetic jets from the fragmentation of the $W^{+*} \rightarrow \bar{q}q$, and two other jets from the $\bar{b}$ and b. Additional information in the event could be supplied by leptonic decay of one of the b quarks, by the observation of a finite flight path for b decay, or by the leptonic decay of the W^{+*} as well as the W^{-*}, resulting in a high p_t (μ^-e^+) or ($\mu^-\mu^+$) pair from different quark decays. These additional features gain in background rejection at a cost in sensitivity. Thus semileptonic decay of the other top costs a factor of five; requiring a lepton from either b is a factor of 2.5, while the price of the finite vertex gap depends on the details of the experimental apparatus—vertex resolution, solid angle coverage, *etc.*

The first search performed by CDF [64] was based on the transverse mass argument used by UA2. The sensitivity reached a slightly higher mass limit because of the larger production cross section, but any search of this type is limited to $m_{top} < M_W$, because if $t \rightarrow Wb$, where W is on shell, then the W transverse mass curve looks normal, and the presence of the top quark would only change the absolute yield of $W \rightarrow e\nu$ by a few percent. More high E_T jet activity is expected from $\bar{p}+p \rightarrow \bar{t}+t$ at 1.8 TeV, so the data sample was restricted to those events with $E_{Te} > 20$ GeV, missing $E_T > 20$ GeV, and two or more jets each with $E_T > 10$ GeV, and $|\eta| < 2$. The transverse mass plot of the 104 events passing these cuts in 4.4 pb^{-1} integrated luminosity is shown in Fig. 31. The data fit expectations from W + jets calculations, consistent with no top quark. The resulting limit was $m_{top} < 77$ GeV/c^2 (95% cl).

The second search of CDF required two high p_t leptons, the lowest background being in the ($\mu^{\pm}, e^{\mp}$) channel [65]. These leptons were assumed to come from the decays $t \rightarrow W^*b$ and $\bar{t} \rightarrow W^*\bar{b}$, where the W's decayed leptonically, and could be off or on shell. This signature was sensitive to top quark masses passing through the threshold for $t \rightarrow W+b$, hence overcoming a defect of the previous technique. Although the event yield is expected to be small because of the dilepton requirement, the backgrounds in this channel are also small, and the signature is easy to understand. The two leptons were required to have $|\eta| < 1.0$ and $E_T > 15$ GeV for electrons, and $|\eta| < 1.2$, $p_{t\mu} > 5$ GeV/c for muons. The 45 opposite sign e-μ events satisfying these criteria are shown in Fig. 32. Monte carlo studies of $b\bar{b}$ and $t\bar{t}$ production indicated that the cluster of events at p_t threshold was consistent with expectations from b decay. Defining the top quark signal region by $E_{Te} > 15$ GeV and $p_{t\mu} > 15$ GeV, 7 events were expected for $m_{top} = 70$ GeV/c. There is one candidate shown in Fig. 32, which led to the limit $m_{top} > 72$ GeV/c^2 (95% cl). The bound obtained from the $e\mu$ channel was statistics limited, and lower than the e^+ jets channel in the same 4.4 pb^{-1} luminosity data sample. The high p_t dilepton signature will be very valuable, however, when higher integrated luminosities are achieved.

The one event in Fig. 32 out all by itself in high (E_t, p_t) space is interesting, but of unknown origin. The information concerning this event is summarized

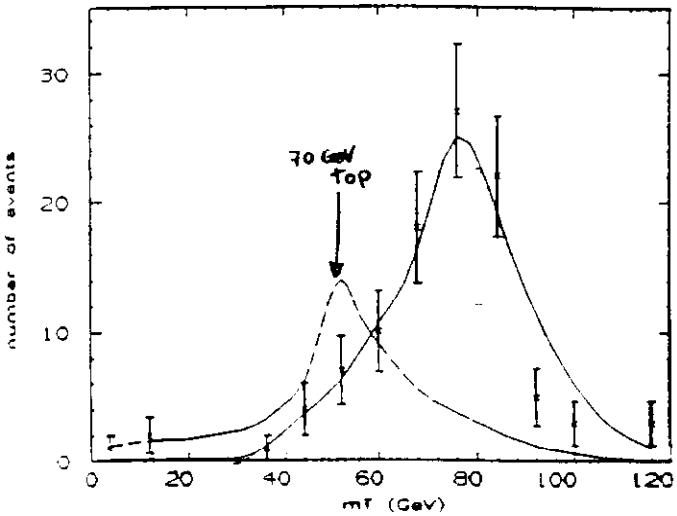

Figure 31: CDF W+ jets transverse mass plot to look for top. The dotted curve shows the signal expected from a 70 GeV/c^2 top.

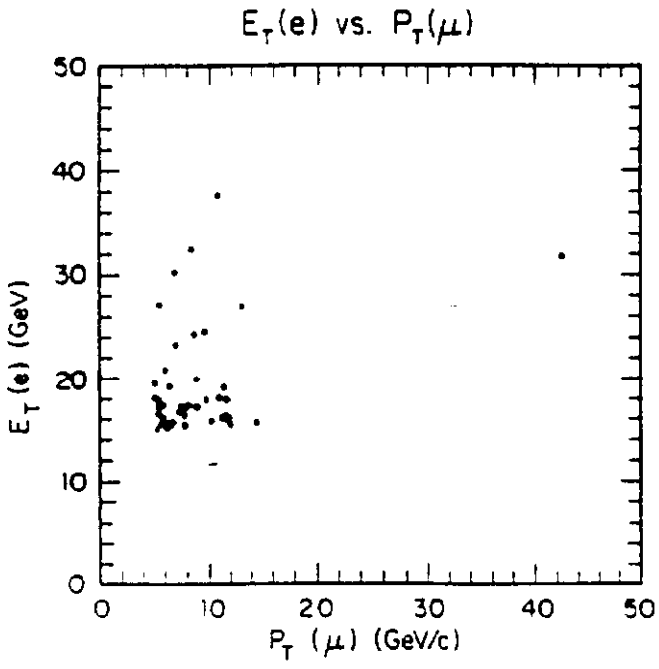

Figure 32: $E_T(e)$ vs $p_t(\mu)$ scatter plot for high transverse momentum $e^{\pm}$, $\mu^{\mp}$ pairs from CDF. One candidate event resides in the top quark search region.

Table 4: High (E_t, p_t) event of Fig. 32

particle	charge	p_t (GeV/c)	η	ϕ (degrees)
central e	+	31.7	−0.81	132
central μ	−	42.5	−0.80	269
forward μ	+	9.9	−2.0	98
jet 1		14	1.1	341
jet 2		5	−2.8	88

in Table 4 [66]. There are three leptons in the event. The reader is welcome to speculate on what it is. More integrated luminosity should explain the mystery.

An update on the CDF analyses, extending the top quark limit to $m_{top} > 89$ GeV, was presented to this Conference by Campagnari [67]. This update was based on two things: a. Extension of the dilepton analysis to e pairs and μ pairs; and b. Extension of the sensitivity of the e + jets search to heavy top mass by looking for daughter muons from b decay in the W+ jets data sample.

The extended dilepton analysis reqired a Z mass window cut 75 GeV/c^2 $< m_{\ell^+\ell^-} <$ 115 GeV/c^2, and missing $E_T > 20$ GeV to suppress backgrounds. In addition the azimuthal separation between the two leptons was required to be $20° < \Delta\phi < 160°$. No further candidates for $t\bar{t}$ decay were found in either the ee or $\mu\mu$ channels, which pushed the limit $m_{top} > 84$ GeV/c^2 (95% cl). This is near the threshold for $t \rightarrow W + b$. This technique has the advantage of having a smoothly varying sensitivity as the threshold is crossed, because it is based on the decay of nearly on shell or on shell W's as m_{top} increases. The threshold is not sharp because of the 2.1 GeV W line width, which is the same order of magnitude as m_b.

The behavior of $t \rightarrow W + b$ near real W threshold has been considered by Gilman and Kaufman [68]. One issue is whether in this region $t \rightarrow W + s$, although suppressed by the CKM matrix, dominates over $t \rightarrow W + b$. The answer is no, because the smoothing effect of the W line width compensates for the discontinuity in decay rates as the W becomes real. Considerations of this nature are relevant in interpreting the other extension described by Campagnari [67], namely the hunt for b quark decays in the W plus jets sample. If $t \rightarrow W + b$ occurs with very little extra energy available in the top quark rest frame, then the b quark will be slow, and the daughter muon will also be slow. In order to maintain sensitivity, the search for muons in the W plus jet sample allowed the muon p_t down to 1.6 GeV/c, a very low threshold value below which the muon would range out in the hadronic calorimeters. To enhance statistics, both the $W \rightarrow e\nu$ sample of Fig. 31 (104 events) and the $W \rightarrow \mu\nu$ + jets sam-

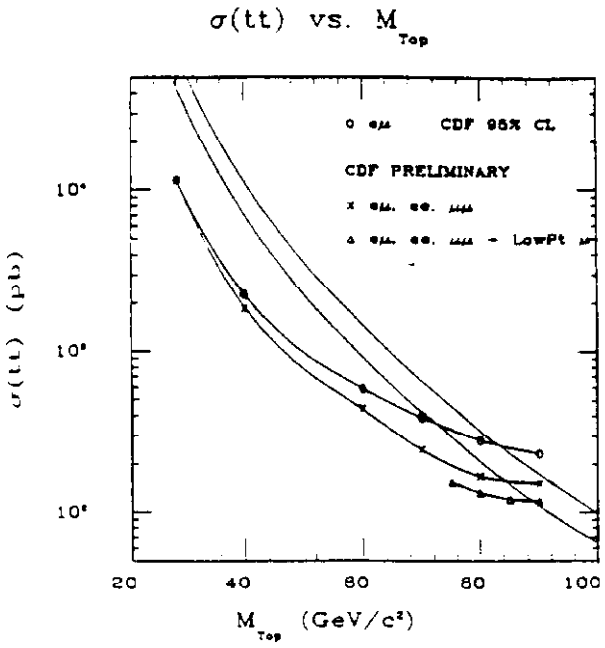

Figure 33: Cross section plot of expected top production showing the preliminary top quark mass limit $m_{\rm top} > 89$ GeV/c^2 from the combined searches in the lepton pair channels and the $W+$ jets channel.

ple of 87 events were used. Seven events were found with muon candidates, but all were within one of the two highest E_T jets in the event. These high E_T jets were presumably from the decay $W \to q\bar{q}$ if the event was indeed $t\bar{t}$ production, and hence the "muons" were background from hadrons in the jets and not daughters of b decay. The b quark jets in these events would be expected to be very low E_T. A minimum separation $\sqrt{\Delta\phi^2 + \Delta\eta^2} > 0.5$ between the muon candidate and either of the two high E_T jets eliminated all seven events. A preliminary value $m_{\rm top} > 89$ GeV/c^2 (95% cl) is quoted in [67]. The CDF results are summarized on the cross section plot of Fig. 33.

4.2.4 *Conclusions of the Top Quark Hunt*

It is clear that the top quark is heavy—too heavy for $Z \to t\bar{t}$ certainly, and probably heavy enough for $t \to W + b$ to occur as a two body decay. The present experimental limits are consistent with the values predicted from Δr, the electroweak radiative correction term, and ΔM, the mass difference in the neutral B system. It is very likely that the signature for $\bar{p}p \to \bar{t}t$ will be the anomalous production of W pairs. Figure 29 shows the top quark cross section at 1.8 TeV out to $m_{\rm top} = 200$ GeV/c^2. The W pair cross section itself in the Standard Model is $\bar{p}p \to W^+W^-X = 10$ pb [69]. Thus $t\bar{t}$ will contribute at least 50% of the total W pair signal out to $m_{\rm top} = 150$ GeV/c^2.

5 Beyond the Standard Model

5.1 *Introduction*

Interest in looking beyond the Standard Model persists even in the absence of any encouraging experimental results. This is quite proper, and essential for progress in the field. The only way to learn anything really new is to discover that the Standard Model is embedded in something larger. The Standard Model does not predict the number of generations of quarks and leptons, and although it is now known that there are three generations of light neutrinos and no more, it is possible that the fourth neutrino is heavy. Heavy lepton searches, both charged and neutral, have been performed at colliders for years [70]. Searches for a fourth generation of quarks, pegged to a charge $-1/3$ b', have run in parallel with the top quark hunts. The neutral Higgs scalar is an integral part of the Standard Model, but is not very easy to find. An entire book is devoted to how to look for it [71]. Beyond the Standard Model one might entertain more massive W's and Z's [72], supersymmetric particles (SUSY) [73], or even something unthinkable.

5.2 *Hadron Colliders Look Beyond*

The first hadron collider searches beyond the Standard Model were made by UA1 [74] and UA2 [75] at the CERN SPS. The first search at the Tevatron by CDF has also been reported [76]. The present situation was summarized at this Conference by Freeman [77].

Most of the effort has concentrated on the high missing transverse energy data sample. This sample was composed in the various experiments of events in which there was substantial jet activity which was not balanced in E_T. In the calorimeters a vector

Table 5: $\not\!\!E_T$ Data Samples

exp	Energy GeV	$L\,dt$ pb^{-1}	$\not\!\!E_T >$ GeV	# jets	$\delta\phi$	# evts	# expected stand mod
UA1	630	0.7	15	2 or >	< 140°	4	5.2 ± 1.9
UA2	630	7.4	40	2 or >	< 160°	none	none
CDF	1800	4.4	40	2 or >	< 150°	98	90 ± 19

missing E_T was defined by the equation

$$\vec{\not\!\!E}_T = -\sum_i E_{Ti}\hat{n}_i, \qquad (54)$$

where $\hat{n}_i$ is a unit vector pointing in the direction of the ith tower. $\not\!\!E_T$, although of great physics interest, is one of the more difficult quantities to measure accurately. Weak towers, dead towers, noisy towers, cracks, cosmic rays, random energy deposits not associated with the beam-beam collision, and simply measurement fluctuations in jet energy all give false $\not\!\!E_T$ signals. After cleanup of obvious garbage, the data samples were restricted to events with large $\not\!\!E_T$. A "significance" defined by

$$S = \not\!\!E_T/\sqrt{E_T} \qquad (55)$$

has been used to characterize the likelihood that the $\not\!\!E_T$ did not come from jet energy fluctuations. The numerator in Eq. (55) is the magnitude of the $\not\!\!E_T$ from Eq. (54), while the denominator is the total scalar E_T. Both CDF and UA1 required $S > 2.8$.

$\not\!\!E_T$ data were used as a signature for possible new physics by identifying all known sources of events, estimating their yield, subtracting them from the sample, and seeing if there was anything of statistical significance left over. Besides energy loss from cracks and measurement fluctuations in QCD jet-jet events, there were such known sources as Z + jets, where $Z \to \nu\bar{\nu}$, and W + jets, where $W \to \tau\nu$, and the tau decayed into a narrow jet, or $W \to e\nu$ or $\mu\nu$ where the charged lepton was lost for some reason.

The resulting data sets are summarized in Table 5. No statistically significant signal unaccounted for by the Standard Model was found. The $\not\!\!E_T$ distribution and jet multiplicity distribution for the CDF data are shown in Figs. 34 a and b.

It is customary to interpret these null results in terms of a minimal SUSY model, because definite conclusions can be drawn regarding mass limits of SUSY particles. An excellent description of the motivation for and consequences of Supersymmetry is given in Ref. [73]. One way to obtain convergence in the radiative corrections to the Higgs

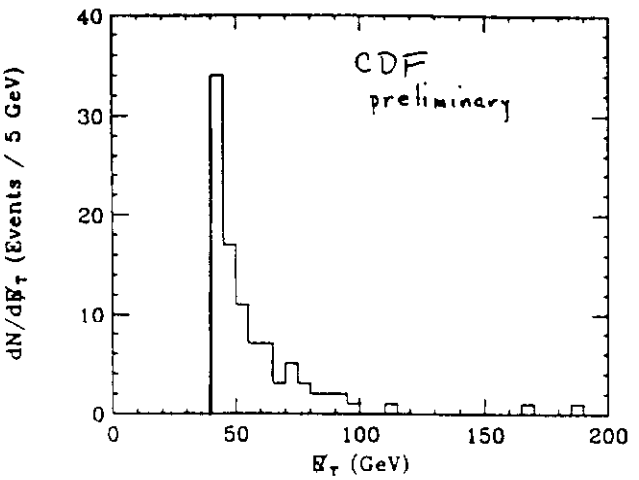

Figure 34a: Missing ET plot from CDF for the candidates selected for the SUSY search.

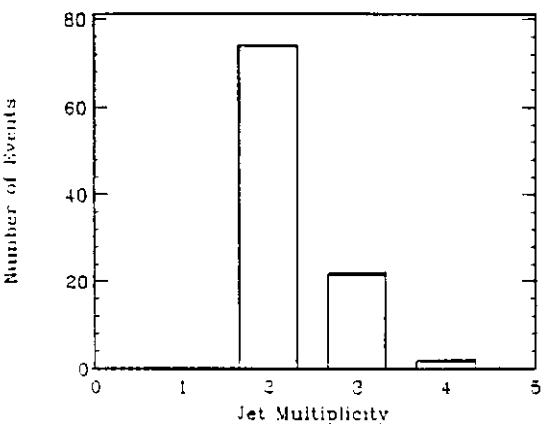

Figure 34b: Jet multiplicity plot for the missing E_T data sample of Fig . 34a.

Table 6: Lower mass limits on squarks and gluinos.

	Squarks	Gluinos
UA1	$M_{\tilde{q}} >$ 45 GeV/c^2	$M_{\tilde{g}} >$ 53 GeV/c^2
UA2	$M_{\tilde{q}} >$ 79 GeV/c^2	$M_{\tilde{g}} >$ 74 GeV/c^2
CDF (prelim.)	$M_{\tilde{q}} >$ 150 GeV/c^2	$M_{\tilde{g}} >$ 150 GeV/c^2

Table 7: Lower mass limits on new gauge bosons.

	W'	Z'
	95% CL	95% CL
UA2	$M_{W'} >$ 209 GeV/c^2	$M_{Z'} >$ 180 GeV/c^2
CDF (prelim.)	$M_{W'} >$ 478 GeV/c^2	$M_{Z'} >$ 380 GeV/c^2

scalar mass is to cancel the loops involving known particles with companion loops of supersymmetric twins, which have all quantum numbers the same except spin. Fermions have SUSY boson partners, and bosons have SUSY fermions. The model introduces a new multiplicative quantum number called R parity which is strictly conserved. All existing particles have $R = +1$, and $R = -1$ for all SUSY partners. This means that SUSY particles, which are strongly interacting and couple to quarks and gluons, must be produced in pairs. For simplicity it is assumed that all squarks have the same mass. There must exist a lightest SUSY particle, or LSP, which is stable. The LSP is usually taken to be the neutral photino. Because the other SUSY particles must be massive or they would have already been discovered, the interaction of photinos with matter, which must involve the creation of a heavy SUSY particle to conserve R, is strongly suppressed by an energy denominator. Hence the photino would appear weakly interacting like a neutrino, and would escape the detector. The signature for SUSY would therefore be large $\not\!\!E_T$ which could not be accounted for by known processes.

There are two scenarios for the heavy SUSY particles. Either a.) $m_{\tilde{g}} > m_{\tilde{q}}$, in which case $\tilde{g} \to \tilde{q}g$, $\tilde{q} \to q\tilde{\gamma}$; or b.) $m_{\tilde{q}} > m_{\tilde{g}}$, in which case $\tilde{q} \to \tilde{g}q$, $\tilde{g} \to q\bar{q}\tilde{\gamma}$. Case (a) leads to a more energetic photino, and hence higher $\not\!\!E_T$ and slightly better mass limits from a null result. Interpreting the data from Table 5 in this way gives the limits in Table 6 [78]. The excluded regions on a $m_{\tilde{q}} - m_{\tilde{g}}$ plot are shown for the preliminary CDF data in Fig. 35.

CDF and UA2 [79] have both searched for heavy W and Z bosons by looking at the high transverse mass data for W's and the high mass lepton pair

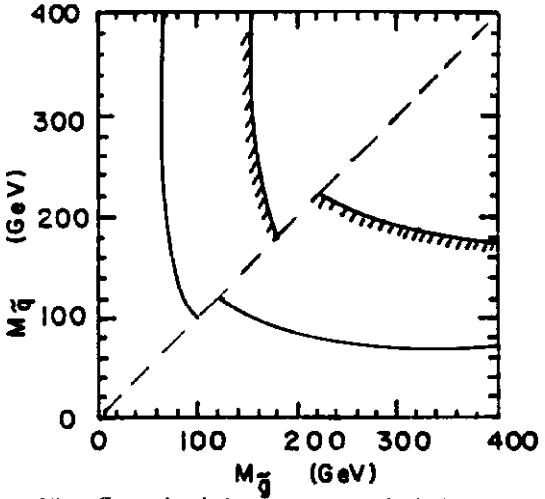

Figure 35: Squark-gluino mass excluded regions. Reference [77] excluded masses below the solid lines, while the higher luminiosity search excludes masses below the hatched lines (CDF Preliminary).

data for Z's. The resulting limits are summarized in Table 7, taken from Ref. [78].

6 Summary and Prospects

In an attempt to measure progress, it is interesting to compare this review to the one performed two years ago by Shochet [80]. Total cross sections and elastic scattering were discussed then, but only extrapolations could be made to 1.8 TeV, where we now have measurements of σ_{TOT} ($\bar{p}p$) and $\frac{d\sigma}{dt}$ at the Tevatron.

The recent high luminosity runs at the SPS and Tevatron have changed the quality of the data on W and Z bosons dramatically. When combined with the e^+e^- measurements on the Z resonance at LEP and the SLC these data can be compared precisely to the predictions of the electroweak theory in a manner which could not have been done two years ago. The theory passes with flying colors. Even radiative corrections to the theory can be tested. These corrections, the experimental limits on m_{TOP}, and the $\bar{B}B$ mass difference are all consistent with a heavy top.

There was evidence that hadron colliders could produce useful samples of b quarks for various studies. This evidence has been confirmed and strengthened, but it is still not known whether hadron colliders will be able to furnish data on this subject of the quality supplied by the e^+e^- colliders. There is

potential there, but not yet really a proof of principle.

The top quark was missing two years ago, and it still is. We now know that the top is a heavy quark, with a mass comparable to or larger than the W/Z masses. This results in a very "top heavy" doublet, since the b quark mass is only 4.5 GeV. A top quark massive enough to decay into a real W has a very short lifetime, too short for toponium to exist as a bound system. The signature for $\bar{p}p \rightarrow \bar{t}t + X$ will be an anomalously large yield of W^+W^- pairs. So far no experiment has presented any convincing evidence of having seen even one W pair. So the future holds many challenges in this area. If $m_{TOP} < 200$ GeV/c^2, then with some luck it will be discovered before the SSC/LHC era begins in 1998.

Supersymmetry mass limits continue to push outward too, and searches for other new physics have not been fruitful either. Here the experimenters must maintain eternal vigilance. A hadron collider detector is not especially user friendly when one is searching for new physics—particularly if the new physics has subtle signatures. There is a lot of background in the data. Nevertheless, there may someday be a real excess in the $\not\!\!E_T$ data, or a peak in the dilepton mass above the Z, or something else which can be experimentally defended but not explained. Keep looking!

7 Acknowledgments

The author wishes to thank his colleagues in the hadron collider collaborations who have contributed so much to our knowledge. He thanks K. K. Phua and Y. Yamaguchi and all of the organizers of the XXV International Conference for the opportunity to give this summary talk, and for the hospitality in Singapore. He thanks Jenny Henderson for her help in assembling this material at the Conference.

References

[1] N.A. Amos *et al.*, *Phys. Lett. B* **243**, 158 (1990).

[2] N.A. Amos *et al.*, *Phys. Rev. Lett.* **61**, 525 (1988).

[3] N.A. Amos *et al.*, *Phys. Rev. Lett.* **63**, 2784 (1989).

[4] D. Bernard *et al.*, *Phys. Lett.* B **198**, 583 (1987).

[5] M.M. Block and R.N. Cahn, *Rev. Mod. Phys.* **57**, 563 (1985).

[6] M.M. Block and R.N. Cahn, *Phys. Lett.* B **188**, 143 (1987).

[7] N.A. Amos *et al.*, *Phys. Lett. B* **247**, 127 (1990).

[8] C. Bourrely, J. Soffer, and T.T. Wu, *Zeit. für Phys. C* **37**, 369 (1988).

[9] This phenomenology is reviewed, for example, by V.D. Barger and D.B. Cline, "Phenomenological Theories of High Energy Scattering", W.A. Benjamin, Inc., New York, 1969.

[10] For a complete account of Pomeranchuk's contributions see "Vospominanya o I. Ya. Pomeranchuke" edited by L.B. Okun, Moscow, 1988.

[11] A. Brandt *et al.*, (UA8 Collaboration), paper contributed to this conference.

[12] A.K. Wroblewski, "Soft Hadron Physics", these Proceedings.

[13] M. Jacob, "Jet Physics and QCD", these Proceedings.

[14] R. Ansari *et al.*, (UA2 Collaboration), *Phys. Lett. B* **186**, 452 (1987).

[15] U. Baur *et al.*, *Phys. Lett. B* **232**, 519 (1989).

[16] Y.K. Kim *et al.*, *Phys. Rev. Lett.* **63**, 1772 (1989).

[17] L. Jones, *Phys. Rev. D* **42**, 811 (1990).

[18] L. Lonnblad, C. Peterson, and T. Rognvaldsson, *Phys. Rev. Lett.* **65**, 1321 (1990).

[19] William J. Marciano and A. Sirlin, *Phys. Rev. D* **29**, 945 (1984), and earlier references therein.

[20] Particle Data Group, *Phys. Lett. B* **204**, 1 (1988).

[21] ibid. p. 102.

[22] F. Dydak, "New Results from e^+e^- at Z_0", these proceedings.

[23] These formulas follow the conventions of M. Consoli, W. Hollik, and F. Jegerlehner, "Z Physics at LEP1", Ed. G. Altarelli, R. Kleiss, and C. Verzegnassi, Vol. 1 CERN 89-08, 1989 (unpublished).

[24] U. Amaldi *et al.*, *Phys. Rev. D* **36**, 1385 (1987); G. Costa *et al.*, Nucl. Phys. B **297**, 244 (1988).

[25] G. Altarelli, *Ann. Rev. Nucl. Part. Sci.* **39**, 357 (1989).

[26] The so far unobserved rare decay $W \to \pi\gamma$ has an interesting theoretical history. An early estimate made by L. Arnellos, W.J. Marciano, and Z. Parsa (*Nucl. Phys. B* **196**, 378 (1982)) was $BR(W \to \pi\gamma) \sim 10^{-9}$. A second calculation by M. Jacob and T.T. Wu (*Phys. Lett. B* **232**, 529 (1989)) indicated that the branching ratio could be much larger—perhaps 10^{-2}. However, that calculation has been questioned by T.N. Pham and X.Y. Pham (*Phys. Lett. B* **247**, 438 (1990)), who obtain a suppression factor $\sim 10^{-4}$ which multiplies the result of Jacob and Wu, thus approaching the original estimate.

[27] J. Alitti *et al.*, (UA2) Collaboration) *Phys. Lett. B* **241**, 150 (1990).

[28] F. Abe *et al.*, (CDF Collaboration) *Phys. Rev. Lett.***65**, 2243 (1990); and *Phys. Rev. D* (to be published).

[29] F. Abe *et al.*, (CDF Collaboration) *Phys. Rev. Lett.* **63**, 720 (1989).

[30] W. Hollik, "Radiative Corrections in the Standard Model", DESY 88-188, 1988 (unpublished).

[31] N. Cabibbo, "Proceedings of the Third Topical Workshop on Proton-Antiproton Collider Physics", CERN 83-04, 567, 1983 (unpublished).

[32] F. Halzen and K. Mursula, *Phys. Rev. Lett.* **51**, 857 (1983).

[33] E.L Berger, F. Halzen, C.S. Kim, and S. Willenbrock, *Phys. Rev. D* **40**, 83 (1989), and references therein.

[34] G. Altarelli, R. K. Ellis, and G. Martinelli, Z. Phys. C **27**, 617 (1985).

[35] F. Halzen and S. Keller, "Proceedings of the Workshop on Hadron Structure Functions and Parton Distributions" Fermilab, 1990 (unpublished).

[36] J-P Revol, these Proceedings. For a description of earlier work by UA1 see C. Albajar *et al.* (UA1 Collaboration), *Z. Phys. C* **44**, 15 (1989).

[37] J. Alitti *et al.* (UA2 collaboration), *Z. Phys. C* **47**, 11 (1990).

[38] F. Abe *et al.* (CDF Collaboration), *Phys. Rev. Lett* **64**, 152 (1990).

[39] R. Marshall, *Rep. Prog. Phys* **52**, 1329 (1989).

[40] T. Kamae, "Proceedings of the XXIV International Conference on High Energy Physics", ed by P. Kotthaus and J. H. Kuhn, Springer Verlag, Berlin, 1989, p 156.

[41] M. Bohm and W. Hollik, "Z Physics at LEP 1", Ed by G. Altarelli, R. Kleiss, and C. Verzegnassi, CERN 89-08 (unpublished), p 205. Our $G_2(s)$ is their $G_3(s)$.

[42] Jonathan L. Rosner, *Phys. Lett. B* **221**, 85 (1989).

[43] J. C. Collins and D. E. Soper, *Phys. Rev. D* **16**, 2219 (1977).

[44] M.E.B. Franklin, these Proceedings.

[45] E. H. Thorndike *et al.* (CLEO Collaboration), High Energy Physics–1980, *Proc. 20th Int. Conf.*, Madison, Wis., ed L. Durand and L. Pondrom, p 105. New York, Am. Inst. Phys. (1981).

[46] E. H. Thorndike and R. A. Poling, *Phys. Rep. 157*, 183 (1988).

[47] C. Albajar *et al.* (UA1 Collaboration) *Phys. Lett. B* **186**, 237(1987).

[48] C. Albajar *et al.* (UA1 Collaboration) *Phys. Lett. B* **213**, 405(1988).

[49] M. Kobayashi and T. Maskawa, *Prog. Theor. Phys* **49**, 652 (1973).

[50] W. Schmidt-Parzefall, *Physics in Collision* **9**, ed J. Grunhaus, p 327. Editions Frontieres, France (1990).

[51] J. Tuominiemi (UA1 Collaboration), these Proceedings.

[52] C. Albajar *et al.* (UA1 Collaboration), *Phys. Lett. B* **186**, 247 (1987).

[53] J. Maalampi and M. Roos, *Particle World* **1**, 110 (1990).

[54] J. L. Hewett, S. Nandi, and T. G. Rizzo, *Phys. Rev.* **D39**, 250 (1989).

[55] C. S. Lim, T. Morozumi, and A. I. Sanda, *Phys. Lett. B* **218**, 343 (1989).

[56] T. Rohaly, these Proceedings.

[57] E.W.N. Glover, A. D. Martin, and W.J. Stirling, *Z. Phys. C* **38**, 473 (1988).

[58] Y. Kubota (CLEO Collaboration), Private Communication.

[59] S. W. Herb *et al.*, *Phys. Rev. Lett.* **39**, 252 (1977).

[60] G. Altarelli, M. Diemoz, G. Martinelli, and P. Nason, *Nucl. Phys. B* **308**, 742 (1988).

[61] C. Albajar *et al.* (UA1 Collaboration), *Z. Phys. C* **37**, 505 (1988).

[62] J-P Revol, these Proceedings. See also C. Albajar *et al.* (UA1 Collaboration), *Z. Phys. C* **48**, 1 (1990).

[63] L. Perini, these Prodeedings. See also T. Akesson *et al.* (UA2 Collaboration), *Z. Phys. C* **46**, 179 (1990).

[64] F. Abe *et al.* (CDF Collaboration), *Phys. Rev. Lett.* **64**, 142 (1990).

[65] F. Abe *et al.* (CDF Collaboration), *Phys. Rev. Lett.* **64**, 147 (1990).

[66] M. Contreras, "Search for the Top Quark in e-μ events in the Collider Detector at Fermilab", PhD Thesis, Brandeis University, 1990 (unpublished).

[67] C. Campagnari, these Proceedings.

[68] Frederick J. Gilman and Russel Kaufman, *Phys. Rev. D* **37**, 2676 (1988).

[69] K. Hagiwara, J. Woodside, and D. Zeppenfeld, *Phys. Rev. D* **41**, 2113 (1990).

[70] C. Albajar *et al.* (UA1 Collaboration), *Phys. Lett.* **B 185**, 233 (1987), and **B 197**, 565 (E) (1987). Searches at e^+e^- colliders are reviewed in Ref. [22] and [39].

[71] J.F. Gunion, H.E. Haber, G. Kane, and S. Dawson, "The Higgs Hunter's Guide", Addison Wesley, New York (1990).

[72] T.G. Rizzo, *Phys. Rev. D* **34**, 1438 (1986); D. London and J. L. Rosner, ibid. p 1530.

[73] H.E. Haber and G.L. Kane, *Phys. Rep* **117**, 75 (1985).

[74] C. Albajar *et al.* (UA1 Collaboration), *Phys. Lett. B* **198**, 261 (1987).

[75] J. Alitti *et al.* (UA2 Collaboration), *Phys. Lett. B* **235**, 363 (1990).

[76] F. Abe *et al.* (CDF Collaboration), *Phys. Rev. Lett* **62**, 1825 (1989).

[77] J. Freeman, these Proceedings

[78] M. Contreras, in "Proceedings of the X International Conference on Physics in Collision", Duke University, 1990 (to be published).

[79] R. Ansari *et al.* (UA2 Collaboration) *Phys. Lett. B* **195**, 613 (1987).

[80] M. J. Shochet, "Proceedings of the XXIV International Conference on High Energy Physics", ed by P. Kotthaus and J. H. Kuhn, Springer Verlag, Berlin, 1989, p 18.